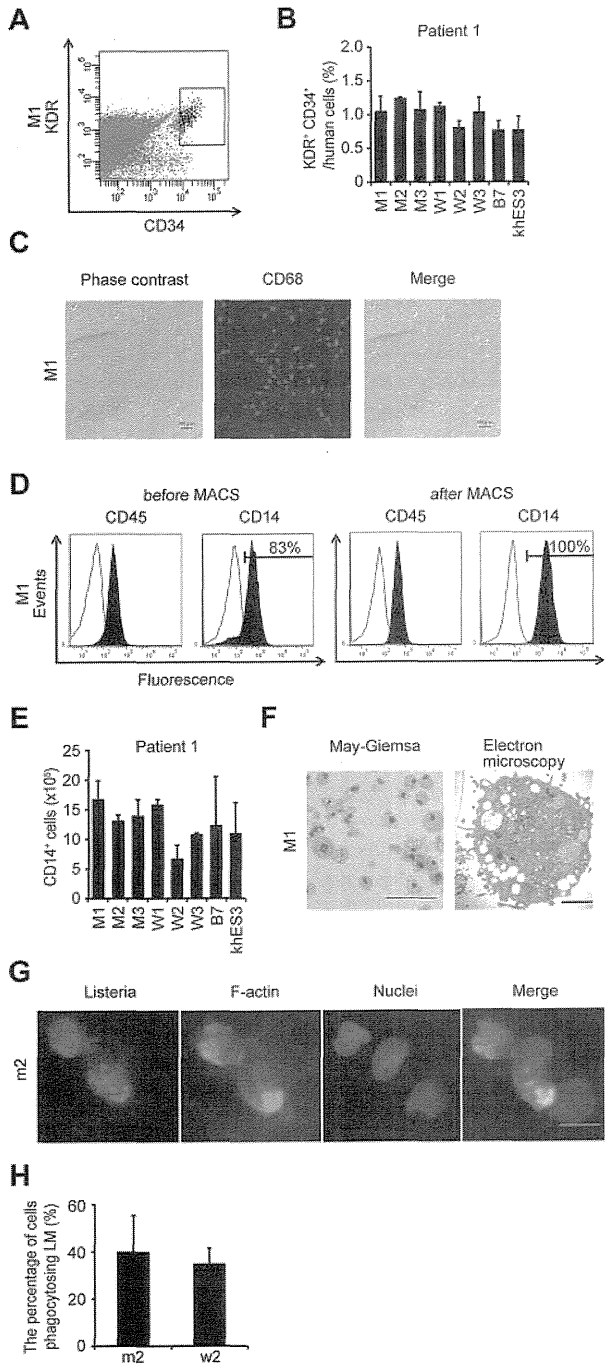

Figure 2. Differentiation and characterization of iPSCs-derived macrophages. (A) KDR$^+$ CD34$^+$ hematopoietic progenitors purified 10 days after differentiation. (B) The percentage of KDR$^+$ CD34$^+$ cells in Tra-1-85$^+$ human cells. n = 3. (C) CD68 immunostaining of macrophages. Scale bars represent 100 μm. (D) The histograms show antibody staining (in black) relative to the isotype-matched controls (in white) for a blood cell marker (CD45), and a macrophage marker (CD14), in cells before (left 2 panels) or after (right 2 panels) magnetic-activated cell sorting purification. (E) CD14$^+$ cell counts obtained from iPSCs plated on an OP9 feeder layer on one 100-mm dish. n = 3. (F) Representative morphology of iPS-MPs evaluated by May-Giemsa staining or transmission electron microscopy. Scale bars represent 100 μm and 2 μm, respectively. (G) The phagocytosis by iPS-MPs after LM infection. The cells were treated with anti-LM antibody, phalloidin, and 4′,6-diamidino-2-phenylindole. Scale bar represents 20 μm. (H) The percentage of iPS-MPs phagocytosing LM was calculated as the average of 9 fields of vision. Data are mean ± SEM.

from the mutant iPS-MPs, the addition of ATP was necessary to induce IL-1β secretion from wild-type iPS-MPs, as it was from either ESC-derived or blood-derived macrophages (Figure 3A). The IL-1β level from mutant iPS-MPs was significantly higher than that from wild-type macrophages, even in the presence of LPS plus ATP. Both groups of macrophages showed similar kinetics in their secretion of other cytokines, such as IL-6 or TNFα (Figure 3A). The results were similar in the iPS-MPs from patient 2 (Figure 3B). Although iPS-MPs showed a similar response at lower LPS concentrations (Figure 3C-D; supplemental Figure 3B-C), no IL-1β secretion was detectable from mutant iPSCs, wild-type iPSCs, or parental fibroblasts in response to stimulation with 1 μg/mL LPS (data not shown). These data demonstrate that the abnormal function of the iPS-MPs is predominantly determined by the *NLRP3* mutation, and not by some unknown genetic alteration(s) prevalent in all cells. We next investigated whether iPS-MPs show pyronecrosis: a pathogen-induced, cathepsin B-dependent, necrosis-like programmed cell death that is characteristically observed in *NLRP3*-mutant monocytes/macrophages.[22,23] When we compared LDH secretion as a marker of membrane rupture, we found that LPS stimulation evoked a significantly higher LDH secretion only from the mutant iPS-MPs, which was inhibited by the cathepsin B inhibitor, CA074Me (Figure 3E).

Despite the low percentage of mutant cells, the clinical manifestation of mosaic CINCA patients is similar to that of patients with a heterozygous mutation.[9,10] We hypothesized that an interaction between the mutant and wild-type macrophages leads to exacerbation of the inflammation. To test this hypothesis, we modeled a mosaic condition by coculturing mutant and wild-type cells. After stimulating mutant iPS-MPs with LPS in separate cultures or in cocultures with wild-type counterparts, we determined the IL-1β level in the supernatant. We found that the IL-1β secretion significantly increased after coculture (Figure 4A; supplemental Figure 4A). Although increasing the cell concentration raised the total amount of the IL-1β secretion from mutants, it did not accelerate the IL-1β secretion per cell from mutant iPS-MPs or enhance the secretion from wild-type macrophages (Figure 4B). To determine the ratio of mutant/wild-type cells at which the additional IL-1β secretion is most enhanced, we changed the ratio using a fixed number of mutant iPS-MPs and increasing the number of wild-type iPS-MPs. We observed a significant increase only at a percentage of 25% mutant macrophages (Figure 4C). Thus, we capitulated, at least in part, the patient's mosaic condition in vitro.

Next, we tried to elucidate whether the interaction is mediated by some humoral factor(s), but supernatant transfer did not facilitate the IL-1β secretion (Figure 4D). As a candidate that may mediate this interaction, we selected ATP because necrotic cells trigger NLRP3-inflammasome activation in part through ATP release.[24] We therefore investigated whether the necrosis-induced ATP secretion activates the wild-type iPS-MPs using ATP receptor antagonists, oxidized ATP (oATP) and PPADS. Although both antagonists markedly inhibited the IL-1β secretion after LPS plus ATP stimulation (supplemental Figure 4B), neither of them abrogated the additional IL-1β secretion in the mixed culture (Figure 4E; compare column 2 with column 3, and column 4 with column 5). The IL-1β secretion from mutant iPS-MPs may have decreased because of off-target effects of oATP.[25] Overall, although it remains to be elucidated how this effect is mediated, these results suggest that the interaction between mutant and wild-type macrophages may enhance IL-1β secretion in mosaic patients.

Validation for future applications for drug screening

An NLRP3-targeted therapeutic approach would be attractive because (1) the progressive arthropathy despite anti–IL-1 therapy indicates that the presence of additional proteins processed by the

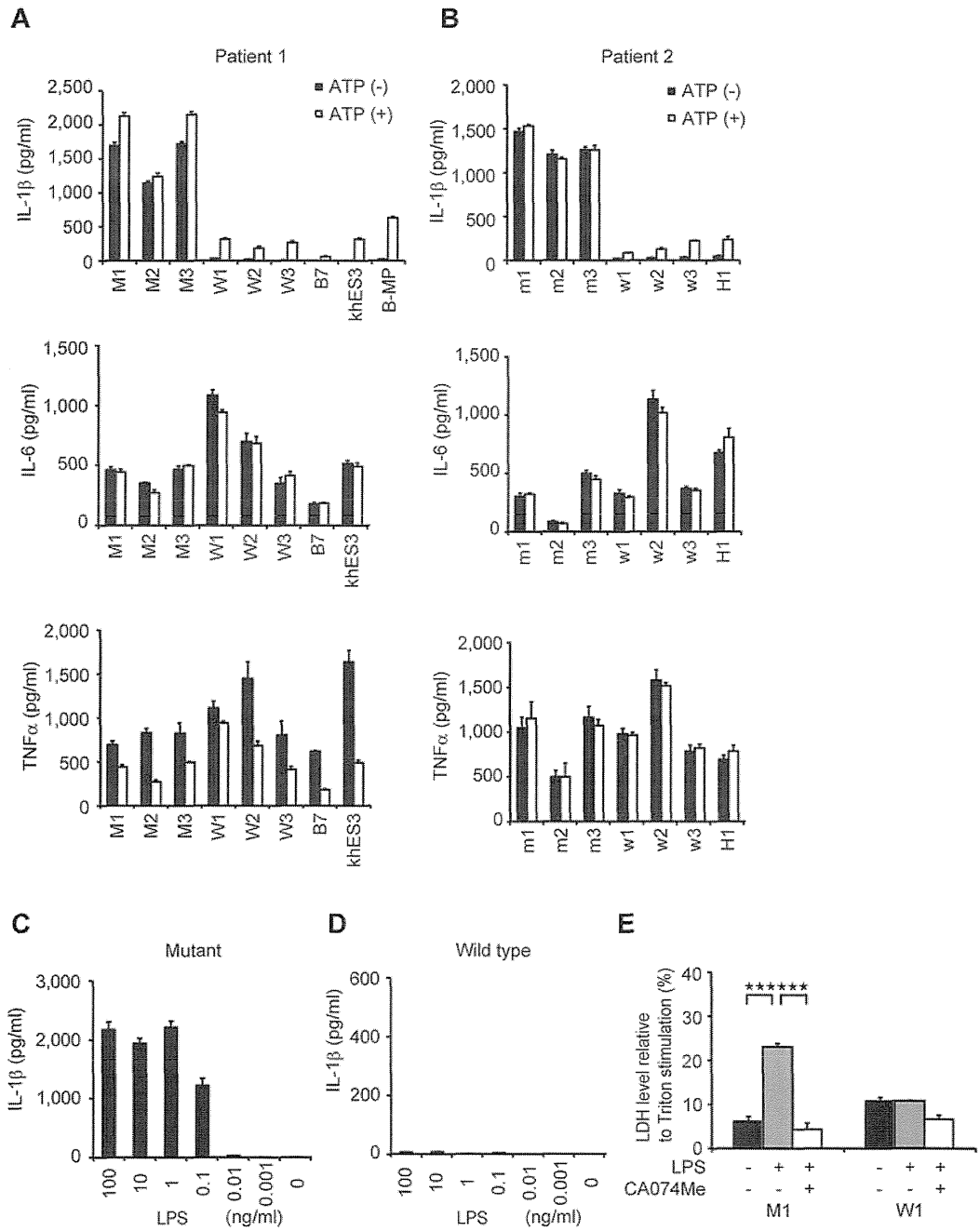

Figure 3. Elucidation of the pathogenesis of somatic mosaic CINCA syndrome. (A) Cytokine secretion from iPS-MPs derived from patient 1. After stimulating iPS-MPs by LPS with or without ATP, we determined the IL-1β (top panel), IL-6 (middle panel), or TNFα (bottom panel) level of the supernatant. n = 3. (B) Cytokine secretion from iPS-MPs derived from patient 2, determined as in panel A. (C) IL-1β secretion from mutant iPS-MPs in the presence of 10-fold dilutions of LPS from 100 ng/mL. n = 3. (D) IL-1β secretion from wild-type iPS-MPs, determined as in panel C. (E) LDH secretion from iPS-MPs stimulated with LPS in the presence or absence of the cathepsin B inhibitor, CA074Me. n = 3. Data are mean ± SEM. ***$P < .001$ (Student t test).

inflammasome is also involved in the pathogenesis of CINCA syndrome; (2) specific inhibition of the NLRP3-inflammasome can avoid unfavorable suppression of other IL-1β–processing pathways in response to various triggers; and (3) these drugs may be also effective for various other NLRP3-related chronic inflammatory conditions, such as Alzheimer disease, diabetes, severe gout, and atherosclerosis.[26-30] Because drug screening using NLRP3 autoactivated cells has not been described previously, we examined whether the iPS-MPs from CINCA patients can serve as a prototype for seeking drug candidates that directly modulate NLRP3-inflammasome activation.

When wild-type iPS-MPs were stimulated with LPS and ATP in the presence of various inhibitors, inhibitors known to modulate molecules upstream of the NLRP3-inflammasome (a protein synthesis inhibitor, cycloheximide, and an NF-κB inhibitor, MG132), downstream of the inflammasome (a caspase-1 inhibitor, Ac-YVAD-CHO), and both upstream of and the inflammasome itself[31] (Bay11-7082) successfully inhibited IL-1β secretion (Figure 5A). Although the precise mechanism is unknown, a cathepsin B inhibitor, CA074Me, also efficiently inhibited IL-1β secretion. As expected, upstream inhibitors inhibited the secretion of other cytokines, such as IL-6 and IL-8, but a downstream inhibitor,

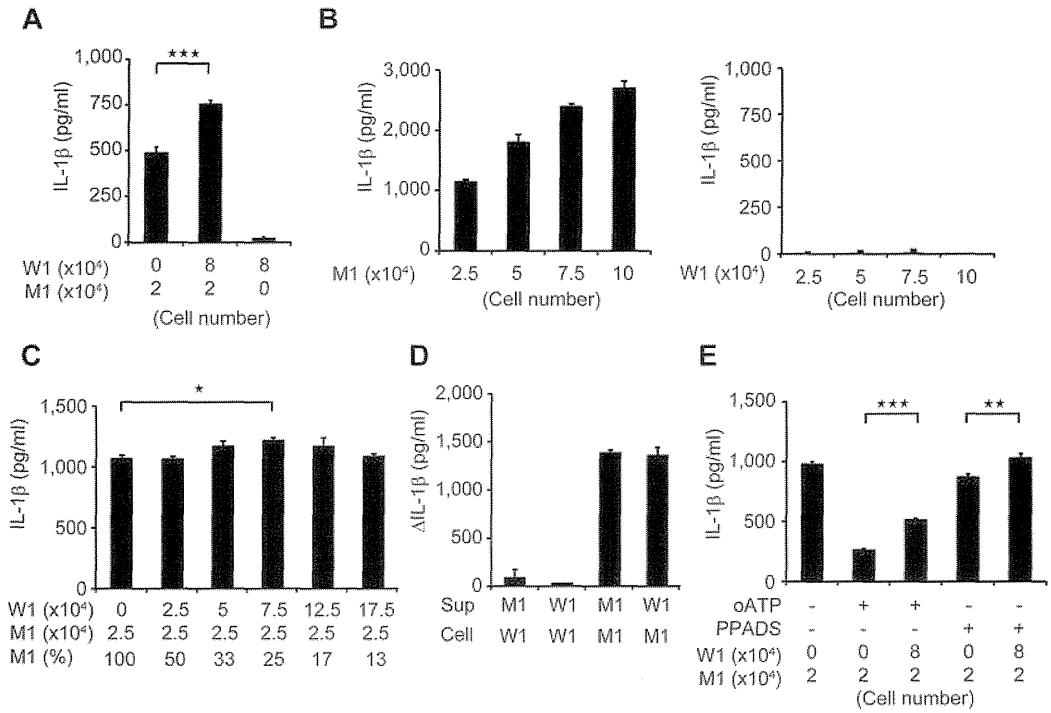

Figure 4. Remodeling mosaicism by coculturing mutant and wild-type iPS-MPs. (A) IL-1β secretion from cocultured iPS-MPs. We used 2 × 10^4 mutant iPS-MPs (M1) and 8 × 10^4 wild-type iPS-MPs (W1) as indicated. n = 6. (B) IL-1β secretion from various numbers of mutant (left panel) or wild-type (right panel) iPS-MPs. The iPS-MPs were seeded at the indicated numbers. n = 3. (C) IL-1β secretion from iPS-MPs that were cocultured at various ratios. The wild-type or mutant iPS-MPs were seeded at the numbers indicated in the first and second rows, respectively. The percentage of mutants is indicated in the third row; n = 3. (D) Increase of IL-1β levels during stimulation by the supernatant. The supernatant was harvested from the wells of the indicated iPS-MPs (Sup) and transferred to the wells of other iPS-MPs (Cell); n = 3. (E) IL-1β secretion from cocultured iPS-MPs in the presence of the ATP receptor antagonist, oATP (300μM) or PPADS (300μM). We used 2 × 10^4 mutant iPS-MPs (M1) and 8 × 10^4 wild-type iPS-MPs (W1) as indicated. n = 6. Data are mean ± SEM. ***$P < .001$ (Student t test). **$P < .01$ (Student t test). *$P < .05$ (Student t test).

Ac-YVAD-CHO, specifically affected IL-1β secretion (Figure 5A). Although CA074Me and Ac-YVAD-CHO inhibited IL-1β secretion regardless of the second signals that were present, PPADS, an inhibitor of extracellular ATP signaling, failed to inhibit IL-1β secretion by following exposure to other second signals, such as monosodium urate and silica crystals (Figure 5B), proving that wild-type iPS-MPs can be activated in a second signal-dependent manner. Therefore, the results of the wild-type iPS-MP-based compound screening depended on the choice of second signals, and such a screening makes it possible to extract candidate compounds that modulate specific second signaling pathways.

Next, we examined the response of mutant iPS-MPs to the inhibitors. In the absence of inhibitors, mutant iPS-MPs secreted a higher level of IL-1β, but treatment with inhibitors dose-dependently decreased IL-1β secretion to the comparable level produced by WT iPS-MPs (Figure 5C). We thus demonstrated the efficacy of these chemical compounds, even for excessive IL-1β production by constitutively hyperactivated inflammasomes. As expected, the mutant iPS-MPs did not respond to PPADS, confirming their autoactivation in a second signal-independent manner (Figure 5D). Therefore, because they can be activated independently from the type of second signals, mutant iPS-MP–based screening would enable the exclusion of compounds that inhibit IL-1β secretion depending on a specific type of second signal transduction. Overall, through using the IL-1β inhibition as the initial criteria and weeding out upstream inhibitors by measuring the levels of other cytokines, we can use *NLRP3*-mutant iPS-MPs to screen for drugs for CINCA syndrome and possibly for other NLRP3-related chronic inflammatory conditions.

Discussion

Since the first identification of a CINCA syndrome patient carrying *NLRP3* mutation as somatic mosaicism,[20] it has been controversial whether the small fraction of *NLRP3*-mutated cells actually causes the strong autoinflammation. It remained unanswered because of the difficulty to separately obtain live mutant and nonmutant blood cells. In this study, we reprogrammed fibroblasts from mosaic patients and obtained macrophages with different genotypes. By showing that only *NLRP3*-mutant iPS-MPs exhibit the distinct proinflammatory phenotype, we demonstrated that the *NLRP3*-mutant macrophages are mainly responsible for the pathogenesis of mosaic CINCA syndrome.

In this study, we established both *NLRP3*-mutant and nonmutant iPSC clones from the same person. One of the potential limitations of studies with patient-derived iPSCs is the difficulty in obtaining isogenic control counterparts, which do not carry the responsible mutations. One possible strategy to solve this problem is to correct the affected gene locus of patient-derived iPSC clones using novel techniques that facilitate homologous recombination.[32,33] As another solution, both affected and control iPSC clones can be obtained from patients of some X-linked hereditary diseases because each iPSC clone originated from somatic cells carrying either a mutated or nonmutated allele as an active X chromosome.[34-36] In the present study, we have retrieved both mutant and wild-type iPSC clones from patients with somatic autosomal mutations. These clones theoretically have the same genetic backgrounds, except for the *NLRP3* gene, and should serve as an ideal pair of mutant and control clones for disease research.

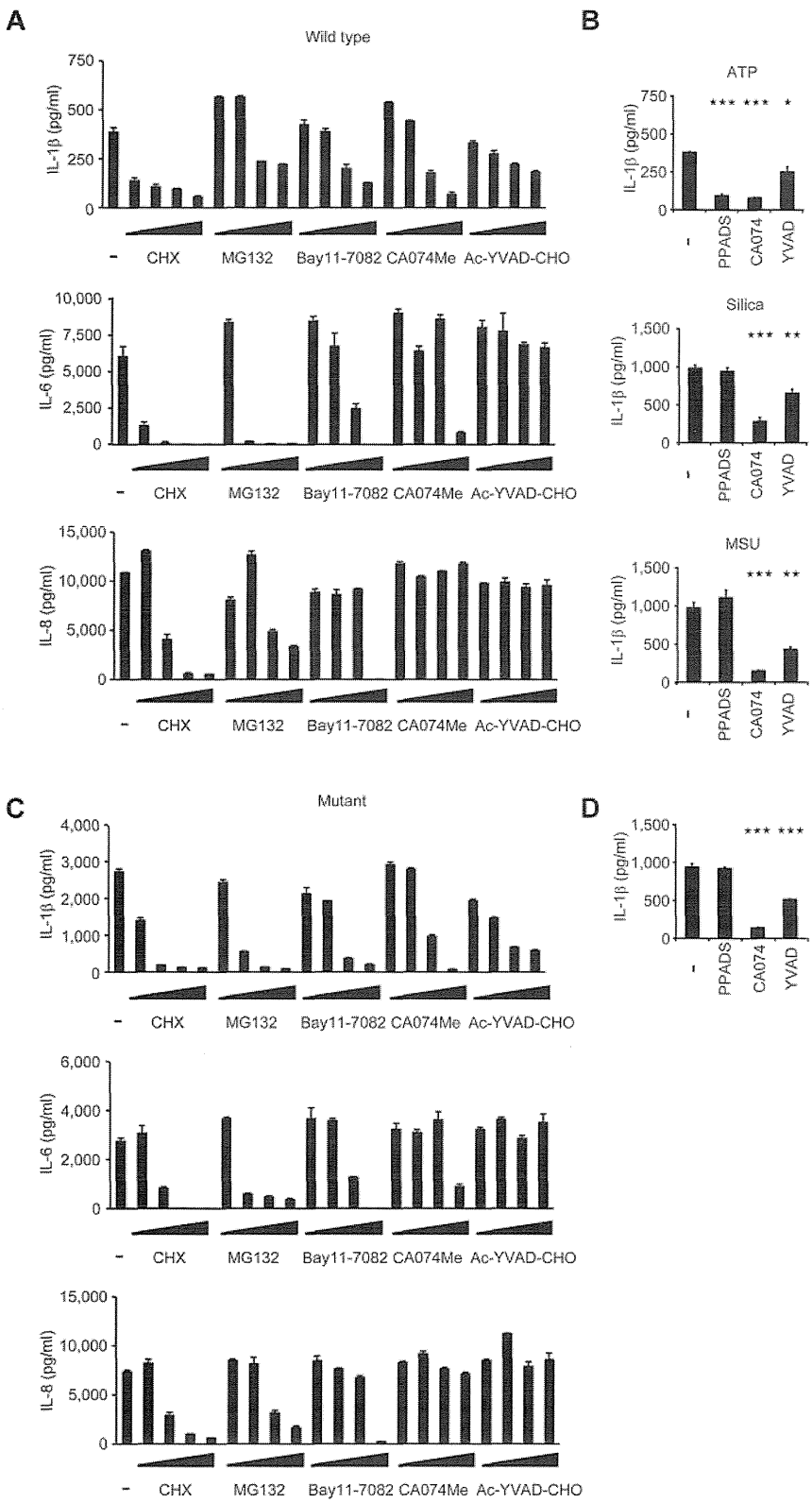

Figure 5. Validation of the cells for future applications for drug screening. (A) Inhibition of IL-1β (top panel), IL-6 (middle panel), or IL-8 (bottom panel) secretion from wild-type iPS-MPs by various inhibitors. The iPS-MPs were cultured for 2 hours in the presence of 100μM cycloheximide (CHX), 100μM MG132, 10μM Bay11-7082, 25μM CA074Me, 50μM Ac-YVAD-CHO, as well as 10-fold dilutions of each inhibitor, except CA074Me (which was diluted 5-fold), followed by LPS treatment plus ATP stimulation. n = 3. (B) The differential inhibition of IL-1β secretion from wild-type iPS-MPs by various inhibitors. In the presence of inhibitors, such as PPADS (300μM), CA074Me (25μM), or Ac-YVAD-CHO (50μM), LPS-primed wild-type iPS-MPs were stimulated with second signal triggers, such as ATP for 1 hour (top panel), silica crystals for 1 hour (middle panel), or monosodium urate crystals for 3 hours (bottom panel). n = 3. (C) Inhibition of IL-1β (top panel), IL-6 (middle panel), or IL-8 (bottom panel) secretion from mutant iPS-MPs by various inhibitors was evaluated as in panel A; n = 3. (D) Inhibition of IL-1β secretion from mutant iPS-MPs by various inhibitors. In the presence of inhibitors, such as PPADS (300μM), CA074Me (25μM), or Ac-YVAD-CHO (50μM), mutant iPS-MPs were stimulated with LPS for 4 hours. n = 3. Data are mean ± SEM. ***$P < .001$ (Student t test). **$P < .01$ (Student t test). *$P < .05$ (Student t test).

In addition to obtaining isogenic controls, iPSCs from patients with somatic autosomal mutations enable dissection and modeling of somatic mosaicism. Despite the fact that each person contains various minor somatic mutations,[37] the effects of mosaicism can often be overlooked because of the difficulty in assessing the possible biologic effects caused by the small cell populations carrying the genetic alterations. Here we dissected somatic mosaicism by obtaining the component cells with heterogeneous genetic identity separately and established an in vitro model to evaluate the interaction between these cells, although precise mechanism of interaction remains to be elucidated. As an approach to determining the disease-causing potential of a specific somatic mutation found in a person, iPSC technology provides advantages compared with ordinary methods, such as the use of transgenic cell lines. First,

iPSCs can be differentiated into the affected cell types or tissues, allowing direct functional assays to be performed that are associated with the pathology. Second, because the disease-causing potential of some mutations is dependent on the genetic backgrounds of the patients,[38] it may be better to obtain both mutant and wild-type clones from a single mosaic patient to more accurately assess the impact of the mutation(s).

Considering that a mutation of *NLRP3* in 10% of the cells is sufficient to cause a distinct disease phenotype, somatic mutations of various genes at an even rarer frequency may also affect the biologic characteristics of a person. Because the presence of the *NLRP3* mutation did not affect the efficacy of reprogramming to the iPSCs, we may be able to obtain both mutant and wild-type iPSC clones from CINCA syndrome patients who carry *NLRP3* mutant cells at a lower percentage. In some diseases, such as Fanconi anemia, however, mutant cells may be resistant to reprogramming.[39,40] Even though there are some possible limitations, establishing both mutant and wild-type iPSC clones is a promising approach to dissect the extent and role of somatic mosaicism.

We demonstrated that several inhibitors that are considered to be effective against CINCA syndrome actually attenuated the disease-relevant phenotype of iPSC-derived macrophages. Before a successful drug screening using iPSC-derived somatic cells can be developed, several limitations need to be overcome, such as the heterogeneity of differentiation and difficulties associated with purification.[18] In this report, we used an efficient and robust differentiation protocol and obtained plenty of macrophages free from the clonal variations.

In conclusion, we elucidated the pathologic roles of both mutant and wild-type cells in mosaic CINCA syndrome patients. After obtaining iPSC-derived macrophages in large quantity and with high purity, we showed they are applicable for drug screening. The iPSC-based approach may help to illuminate the pathogenesis of various diseases that are caused by somatic mosaicism, and facilitate drug discovery for the treatment of NLRP3-related inflammatory diseases.

Acknowledgments

The authors thank the CINCA syndrome patients who participated in this study; Y. Sasaki, Y. Jindai, A. Okada, M. Narita, A. Nagahashi, T. Ohkame, S. Nishimoto, Y. Inoue, and S. Arai for technical assistance; I. Kato for help with animal experiments; M. Nakagawa, K. Okita, Y. Yoshida, T. Aoi, and M. Yanagimachi for scientific comments; and R. Kato, E. Nishikawa, S. Takeshima, Y. Otsu, H. Hasaba, H. Watanabe, T. Ishii, H. Kurokawa, N. Takasu, and Y. Takao for administrative assistance.

This work was supported by the Ministry of Health, Labor and Welfare (N.M. and T.N.), the Ministry of Education, Culture, Sports, Science and Technology (MEXT; N.M. and T.N.), the Leading Project of MEXT (S.Y. and T.N.), the Promotion of Fundamental Studies in Health Sciences of National Institute of Biomedical Innovation (S.Y.), the Funding Program for World-Leading Innovative Research and Development on Science and Technology (FIRST Program) of Japan Society for the Promotion of Science (JSPS; T.N., and S.Y.), JSPS and MEXT (Grants-in-Aid for Scientific Research; S.Y.), JSPS (T.N., T.T., and M.K.S.), the Takeda Science Foundation, SENSHIN Medical Research Foundation, and Suzuken Memorial Foundation to (M.K.S.).

Authorship

Contribution: T.T. planned the project, established iPSCs, performed experimental work, analyzed data, and prepared the manuscript; K.T. planned the project, established iPSCs, and analyzed data; M.Y., S.T., and S.N. performed experimental work; K.O., A.N., and T.H. analyzed data; R.N. and N.K. planned the project; H.H. and M.M. performed *L monocytogenes* infection; N.M. and J.E.H. performed electron microscopy; T.Y. identified retroviral integration sites; A.W. performed bisulfite sequencing; A.S.-O. and S.O. analyzed CNV; I.A. established iPSCs; S.Y. and T.N. planned the project and analyzed data; M.K.S. planned the project, analyzed data, and prepared the manuscript; and all authors read and approved the manuscript.

Conflict-of-interest disclosure: S.Y. is a member without salary of the scientific advisory boards of iPierian, iPS Academia Japan, and Megakaryon Corporation. The remaining authors declare no competing financial interests.

Correspondence: Megumu K. Saito, Center for iPS Cell Research and Application, Kyoto University, Kyoto 606-8507, Japan; e-mail: msaito@cira.kyoto-u.ac.jp.

References

1. Prieur AM, Griscelli C, Lampert F, et al. A chronic, infantile, neurological, cutaneous and articular (CINCA) syndrome: a specific entity analysed in 30 patients. *Scand J Rheumatol Suppl.* 1987;66: 57-68.
2. Aksentijevich I, Nowak M, Mallah M, et al. De novo CIAS1 mutations, cytokine activation, and evidence for genetic heterogeneity in patients with neonatal-onset multisystem inflammatory disease (NOMID): a new member of the expanding family of pyrin-associated autoinflammatory diseases. *Arthritis Rheum.* 2002;46(12):3340-3348.
3. Feldmann J, Prieur AM, Quartier P, et al. Chronic infantile neurological cutaneous and articular syndrome is caused by mutations in CIAS1, a gene highly expressed in polymorphonuclear cells and chondrocytes. *Am J Hum Genet.* 2002;71(1):198-203.
4. Bauernfeind FG, Horvath G, Stutz A, et al. Cutting edge: NF-kappaB activating pattern recognition and cytokine receptors license NLRP3 inflammasome activation by regulating NLRP3 expression. *J Immunol.* 2009;183(2):787-791.
5. Mariathasan S, Weiss DS, Newton K, et al. Cryopyrin activates the inflammasome in response to toxins and ATP. *Nature.* 2006; 440(7081):228-232.
6. Gattorno M, Tassi S, Carta S, et al. Pattern of interleukin-1beta secretion in response to lipopolysaccharide and ATP before and after interleukin-1 blockade in patients with CIAS1 mutations. *Arthritis Rheum.* 2007;56(9):3138-3148.
7. Goldbach-Mansky R, Dailey NJ, Canna SW, et al. Neonatal-onset multisystem inflammatory disease responsive to interleukin-1beta inhibition. *N Engl J Med.* 2006;355(6):581-592.
8. Neven B, Marvillet I, Terrada C, et al. Long-term efficacy of the interleukin-1 receptor antagonist anakinra in ten patients with neonatal-onset multisystem inflammatory disease/chronic infantile neurologic, cutaneous, articular syndrome. *Arthritis Rheum.* 2010;62(1):258-267.
9. Saito M, Nishikomori R, Kambe N, et al. Disease-associated CIAS1 mutations induce monocyte death, revealing low-level mosaicism in mutation-negative cryopyrin-associated periodic syndrome patients. *Blood.* 2008;111(4):2132-2141.
10. Tanaka N, Izawa K, Saito MK, et al. High incidence of NLRP3 somatic mosaicism in patients with chronic infantile neurologic, cutaneous, articular syndrome: results of an International Multicenter Collaborative Study. *Arthritis Rheum.* 2011;63(11):3625-3632.
11. Masters SL, Simon A, Aksentijevich I, Kastner DL. Horror autoinflammaticus: the molecular pathophysiology of autoinflammatory disease. *Annu Rev Immunol.* 2009;27:621-668.
12. Youssoufian H, Pyeritz RE. Mechanisms and consequences of somatic mosaicism in humans. *Nat Rev Genet.* 2002;3(10):748-758.
13. Erickson RP. Somatic gene mutation and human disease other than cancer: an update. *Mutat Res.* 2010;705(2):96-106.
14. Ariga T, Kondoh T, Yamaguchi K, et al. Spontaneous in vivo reversion of an inherited mutation in the Wiskott-Aldrich syndrome. *J Immunol.* 2001; 166(8):5245-5249.

15. Nishikomori R, Akutagawa H, Maruyama K, et al. X-linked ectodermal dysplasia and immunodeficiency caused by reversion mosaicism of NEMO reveals a critical role for NEMO in human T-cell development and/or survival. *Blood.* 2004; 103(12):4565-4572.
16. Lutskiy MI, Beardsley DS, Rosen FS, Remold-O'Donnell E. Mosaicism of NK cells in a patient with Wiskott-Aldrich syndrome. *Blood.* 2005;106(8):2815-2817.
17. Takahashi K, Tanabe K, Ohnuki M, et al. Induction of pluripotent stem cells from adult human fibroblasts by defined factors. *Cell.* 2007;131(5): 861-872.
18. Grskovic M, Javaherian A, Strulovici B, Daley GQ. Induced pluripotent stem cells: opportunities for disease modelling and drug discovery. *Nat Rev Drug Discov.* 2011;10(12):915-929.
19. Hanna J, Markoulaki S, Schorderet P, et al. Direct reprogramming of terminally differentiated mature B lymphocytes to pluripotency. *Cell.* 2008;133(2): 250-264.
20. Saito M, Fujisawa A, Nishikomori R, et al. Somatic mosaicism of CIAS1 in a patient with chronic infantile neurologic, cutaneous, articular syndrome. *Arthritis Rheum.* 2005;52(11):3579-3585.
21. Nakano T, Kodama H, Honjo T. Generation of lymphohematopoietic cells from embryonic stem cells in culture. *Science.* 1994;265(5175):1098-1101.
22. Fujisawa A, Kambe N, Saito M, et al. Disease-associated mutations in CIAS1 induce cathepsin B-dependent rapid cell death of human THP-1 monocytic cells. *Blood.* 2007;109(7):2903-2911.
23. Willingham SB, Bergstralh DT, O'Connor W, et al. Microbial pathogen-induced necrotic cell death mediated by the inflammasome components CIAS1/cryopyrin/NLRP3 and ASC. *Cell Host Microbe.* 2007;2(3):147-159.
24. Iyer SS, Pulskens WP, Sadler JJ, et al. Necrotic cells trigger a sterile inflammatory response through the Nlrp3 inflammasome. *Proc Natl Acad Sci U S A.* 2009;106(48):20388-20393.
25. Beigi RD, Kertesy SB, Aquilina G, Dubyak GR. Oxidized ATP (oATP) attenuates proinflammatory signaling via P2 receptor-independent mechanisms. *Br J Pharmacol.* 2003;140(3):507-519.
26. Martinon F, Petrilli V, Mayor A, Tardivel A, Tschopp J. Gout-associated uric acid crystals activate the NALP3 inflammasome. *Nature.* 2006; 440(7081):237-241.
27. Halle A, Hornung V, Petzold GC, et al. The NALP3 inflammasome is involved in the innate immune response to amyloid-beta. *Nat Immunol.* 2008;9(8):857-865.
28. Duewell P, Kono H, Rayner KJ, et al. NLRP3 inflammasomes are required for atherogenesis and activated by cholesterol crystals. *Nature.* 2010; 464(7293):1357-1361.
29. Masters SL, Dunne A, Subramanian SL, et al. Activation of the NLRP3 inflammasome by islet amyloid polypeptide provides a mechanism for enhanced IL-1beta in type 2 diabetes. *Nat Immunol.* 2010;11(10):897-904.
30. Vandanmagsar B, Youm YH, Ravussin A, et al. The NLRP3 inflammasome instigates obesity-induced inflammation and insulin resistance. *Nat Med.* 2011;17(2):179-188.
31. Juliana C, Fernandes-Alnemri T, Wu J, et al. Anti-inflammatory compounds parthenolide and Bay 11-7082 are direct inhibitors of the inflammasome. *J Biol Chem.* 2010;285(13):9792-9802.
32. Aizawa E, Hirabayashi Y, Iwanaga Y, et al. Efficient and accurate homologous recombination in hESCs and hiPSCs using helper-dependent adenoviral vectors. *Mol Ther.* 2012;20(2):424-431.
33. Soldner F, Laganiere J, Cheng AW, et al. Generation of isogenic pluripotent stem cells differing exclusively at two early onset Parkinson point mutations. *Cell.* 2011;146(2):318-331.
34. Cheung AY, Horvath LM, Grafodatskaya D, et al. Isolation of MECP2-null Rett syndrome patient hiPS cells and isogenic controls through X-chromosome inactivation. *Hum Mol Genet.* 2011;20(11):2103-2115.
35. Kim KY, Hysolli E, Park IH. Neuronal maturation defect in induced pluripotent stem cells from patients with Rett syndrome. *Proc Natl Acad Sci U S A.* 2011;108(34):14169-14174.
36. Pomp O, Dreesen O, Leong DF, et al. Unexpected X chromosome skewing during culture and reprogramming of human somatic cells can be alleviated by exogenous telomerase. *Cell Stem Cell.* 2011;9(2):156-165.
37. Gore A, Li Z, Fung HL, et al. Somatic coding mutations in human induced pluripotent stem cells. *Nature.* 2011;471(7336):63-67.
38. Crotti L, Lundquist AL, Insolia R, et al. KCNH2-K897T is a genetic modifier of latent congenital long-QT syndrome. *Circulation.* 2005;112(9): 1251-1258.
39. Raya A, Rodriguez-Piza I, Guenechea G, et al. Disease-corrected haematopoietic progenitors from Fanconi anemia induced pluripotent stem cells. *Nature.* 2009;460(7251):53-59.
40. Müller LU, Milsom MD, Harris CE, et al. Overcoming reprogramming resistance of Fanconi anemia cells. *Blood.* 2012;119(23):5449-5457.

Frequent somatic mosaicism of *NEMO* in T cells of patients with X-linked anhidrotic ectodermal dysplasia with immunodeficiency

Tomoki Kawai,[1] Ryuta Nishikomori,[1] Kazushi Izawa,[1] Yuuki Murata,[1] Naoko Tanaka,[1] Hidemasa Sakai,[1] Megumu Saito,[2] Takahiro Yasumi,[1] Yuki Takaoka,[1] Tatsutoshi Nakahata,[2] Tomoyuki Mizukami,[3] Hiroyuki Nunoi,[3] Yuki Kiyohara,[4] Atsushi Yoden,[5] Takuji Murata,[5] Shinya Sasaki,[6] Etsuro Ito,[6] Hiroshi Akutagawa,[7] Toshinao Kawai,[8] Chihaya Imai,[9] Satoshi Okada,[10] Masao Kobayashi,[10] and Toshio Heike[1]

[1]Department of Pediatrics, Kyoto University Graduate School of Medicine, Kyoto, Japan; [2]Clinical Application Department, Center for iPS Cell Research and Application, Institute for Integrated Cell-Material Sciences, Kyoto University, Kyoto, Japan; [3]Division of Pediatrics, Department of Reproductive and Developmental Medicine, Faculty of Medicine, University of Miyazaki, Miyazaki, Japan; [4]Department of Pediatrics, Faculty of Medicine, Osaka University, Suita, Japan; [5]Department of Pediatrics, Osaka Medical College, Takatsuki, Japan; [6]Department of Pediatrics, Hirosaki University Graduate School of Medicine, Hirosaki, Japan; [7]Department of Pediatrics, Kishiwada City Hospital, Kishiwada, Japan; [8]Department of Human Genetics, National Center for Child Health and Development, Tokyo, Japan; [9]Department of Pediatrics, Niigata University, Niigata, Japan; and [10]Department of Pediatrics, Hiroshima University Graduate School of Biomedical Sciences, Hiroshima, Japan

Somatic mosaicism has been described in several primary immunodeficiency diseases and causes modified phenotypes in affected patients. X-linked anhidrotic ectodermal dysplasia with immunodeficiency (XL-EDA-ID) is caused by hypomorphic mutations in the *NF-κB essential modulator (NEMO)* gene and manifests clinically in various ways. We have previously reported a case of XL-EDA-ID with somatic mosaicism caused by a duplication mutation of the *NEMO* gene, but the frequency of somatic mosaicism of *NEMO* and its clinical impact on XL-EDA-ID is not fully understood. In this study, somatic mosaicism of *NEMO* was evaluated in XL-EDA-ID patients in Japan. Cells expressing wild-type NEMO, most of which were derived from the T-cell lineage, were detected in 9 of 10 XL-EDA-ID patients. These data indicate that the frequency of somatic mosaicism of *NEMO* is high in XL-ED-ID patients and that the presence of somatic mosaicism of *NEMO* could have an impact on the diagnosis and treatment of XL-ED-ID patients. (*Blood.* 2012;119(23):5458-5466)

Introduction

X-linked anhidrotic ectodermal dysplasia with immunodeficiency (XL-EDA-ID) is a disease with clinical features including hypohidrosis, delayed eruption of teeth, coarse hair, and immunodeficiency associated with frequent bacterial infections.[1-5] The gene responsible for XL-EDA-ID has been identified as *NF-κB essential modulator (NEMO).*[6-8] NEMO is necessary for the function of IκB kinase, which phosphorylates and degrades IκB to activate NF-κB.[9-10] Defects in NEMO cause various abnormalities in signal transduction pathways involving NF-κB, and affect factors such as the IL-1 family protein receptors, the TLRs, VEGFR-3, receptor activator of nuclear factor κB (RANK), the ectodysplasin-A receptor, CD40, and the TNF receptor I.[7] Whereas a complete loss of NEMO function in humans is believed to cause embryonic lethality,[11] *NEMO* mutations in XL-EDA-ID patients are hypomorphic,[8] causing a partial loss of NEMO functions.

In XL-EDA-ID, NEMO defects lead to diverse immunologic features including susceptibility to pathogens, impaired Ab response to polysaccharides,[2,4,12] hypogammaglobulinemia,[13] hyper IgM syndrome,[14] and impaired NK-cell activity,[15] with a large degree of variability in phenotypes among the patients. For example, approximately one-tenth of XL-EDA-ID patients exhibit reduced mitogen-induced proliferation of T lymphocytes.[12] Moreover, one-fourth suffer from inflammatory disorders such as inflammatory bowel disease and rheumatoid arthritis,[12] although the inflammatory process usually relies on NF-κB activation.[16] One explanation for this clinical variability is that the XL-EDA-ID phenotype is *NEMO* genotype-specific. Although the XL-EDA-ID database reported by Hanson et al succeeds to some extent in linking the specific clinical features to *NEMO* genotype,[12] the penetrance of some clinical features is not high and the mechanism accounting for this variability is unknown.

Recently, we have reported a case of spontaneous reversion mosaicism of the *NEMO* gene in XL-EDA-ID, which showed an atypical phenotype involving decreased mitogen-induced T-cell proliferation along with decreased CD4 T cells (patient 1).[17] There have been no subsequent reports on somatic mosaicism in XL-EDA-ID, and its prevalence and impact on the clinical features of the disease is unknown. In this study, we describe the younger brother of patient 1, who suffered from XL-EDA-ID with the same mutation and somatic reversion mosaicism of *NEMO*. Patient 2 showed intriguing laboratory findings in that mitogen-induced T-cell proliferation varied in accordance with the rate of detected reversion in the peripheral blood. These 2 cases led us to perform a nationwide study of XL-EDA-ID patients in Japan that revealed a high incidence of somatic mosaicism of *NEMO*.

Submitted May 11, 2011; accepted April 8, 2012. Prepublished online as *Blood* First Edition paper, April 19, 2012; DOI 10.1182/blood-2011-05-354167.

The online version of this article contains a data supplement.

The publication costs of this article were defrayed in part by page charge payment. Therefore, and solely to indicate this fact, this article is hereby marked "advertisement" in accordance with 18 USC section 1734.

Table 1. Clinical and genetic features of XL-EDA-ID patients

Patient	Mutation	Ectodermal dysplasia	Mitogen-induced proliferation	Infections	Complications	Therapy	Sex chromosome chimerism
1	Duplication	+	Reduced	Sepsis (S.P. and P.A.) Disseminated M.A.C. Skin abscess (S.A.) Invasive *Aspergillus*	Chronic diarrhea Failure to thrive Small intestinal stenosis Lymphedema	IVIG RFP, CAM, AMK, EB Rifabutin	100% XY
2	Duplication	+	Reduced	Sepsis (*E coli*) Disseminated M.S.	Failure to thrive	IVIG, ST, EB, CAM Rifabutin, SCT	99.8% XY 0.2% X
3	D311E	−	Normal	Disseminated B.C.G. Sepsis (S.P.)		IVIG, INH RFP, SCT	100% XY
4	A169P	+	Normal	Meningitis (S.P.)	IBD Interstitial pneumonia Rheumatoid arthritis	IVIG, ST, PSL CyA, MTX, Infliximab	99% XY
5	L227P	+	Normal	Recurrent pneumonia Pyogenic coxitis Recurrent otitis media	IBD	ST, mesalazine Infliximab	Not done
6	R182P	+	Not done	Recurrent otitis media UTI, Recurrent stomatitis Subepidermal abscess	IBD	ST, mesalazine	99.8% XY 0.2% X
7	R175P	+	Normal	Recurrent sepsis (S.P.)		IVIG	100% XY
8	Q348X	+	Normal	Disseminated B.C.G.	IBD	IVIG, ST	100% XY
9	R175P	+	Normal	Recurrent pneumonia Recurrent otitis media Kaposi varicelliform eruption	IBD	IVIG 5-aminosalicylic acid	100% XY
10	1167 ins C	+	Normal	Sepsis and Enteritis (E.A) Sepsis (C.G.) UTI (K.P.)	Failure to thrive Pyloric stenosis, colon polyps	IVIG, SCT	Not done

S.P. indicates *Streptococcus pneumoniae*; P.A., *Pseudomonas aeruginosa*; IVIG, intravascular immunoglobulin infusion; M.A.C., *Mycobacterium avium* complex; S.A., *Staphylococcus aureus*; *E coli*, *Escherichia coli*; ST, trimethoprim-sulfamethoxazole; M.S., *Mycobacterium szulgai*; AMK, amikacin; EB, ethambutol; CAM, clarithromycin; SCT, stem cell transplantation; B.C.G., Bacille de Calmette et Guerin; INH, isoniazid; RFP, rifampicin; IBD, inflammatory bowel disease; PSL, prednisolone; CyA, cyclosporine A; MTX, methotrexate; UTI, urinary tract infection; E.A., *Enterobacter aerogenes*; C.G., *Candida glabrata*; and K.P., *Klebsiella* pneumonia.

Methods

Informed consent

Informed consent was obtained from the patients and their families following the Declaration of Helsinki according to the protocol of the Internal Review Board of Kyoto University, which approved this study.

Patients

Patient 1 was an XL-EDA-ID patient with a duplication mutation of the *NEMO* gene spanning intron 3 to exon 6. This patient has been reported previously[17] and died from an *Aspergillus* infection at the age of 4. Patient 2, born at term, was the younger brother of patient 1. This patient was also diagnosed as XL-EDA-ID with the same duplication mutation as patient 1 by genetic study. He received trimethoprim-sulfamethoxazole prophylaxis and a monthly infusion of immunoglobulin from the age of 1 month. The patient maintained good health and had a body weight of 7899*g* at 6 months when he started to fail to thrive. Except for poor weight gain, patient 2 appeared active with a good appetite, negative C-reactive protein, normal white blood cell counts, and no apparent symptoms. At 19 months of age, *Mycobacterium szulgai* was detected by venous blood culture, and the patient was treated with multidrug regimens including ethambutol, rifabutin, and clarithromycin based on the treatment of systemic *Mycobacterium avium* complex infection. The patient responded well to the treatment and his weight increased from 7830*g* to 9165*g* within a month after the treatment was initiated. Patient 2 received an unrelated cord blood cell transplantation at 26 months of age, containing 8.5×10^7 nucleated cells/kg (4.4×10^5 $CD34^+$ cells/kg), which was matched at 5 of 8 loci: mismatches occurred at 1 HLA-B and 1 HLA-C allele (according to serology), and at 1 HLA-A, 1 HLA-B, and 1 HLA-C allele (according to DNA typing). The preconditioning regimen consisted of fludarabine (30 mg/m^2/d) on days −7 to −3, melphalan (70 mg/m^2/d) on days −6 to −5, and rabbit anti-thymocyte globulin (2.5 mg/kg/d) on days −6 to −2. At first, Tacrolimus (0.024 mg/kg/d) was used to prevent GVHD, but this was switched to cyclosporin A (3 mg/kg/d) on day 9 because of drug-induced encephalopathy. Neutrophil ($> 0.5 \times 10^9$/L) and platelet ($> 50 \times 10^9$/L) engraftment were examined on days 13 and 40, respectively. Although $CD19^+$ cells (2042/μL, 94% donor chimerism), $CD56^+$ cells (242/μL, 97% donor chimerism), and monocytes (557/μL, 69% donor chimerism) were successfully generated, $CD3^+$ cells were not detected in the peripheral blood by day 54. The patient suffered from septic shock and died on day 60. Patients 3 to 10 were XL-EDA-ID patients recruited nationwide in Japan. Clinical details of patients 3, 4, and 10 have been reported previously.[18-20] These patients had clinical phenotypes characteristic of XL-EDA-ID such as ectodermal dysplasia, innate and/or acquired immunity defects, and susceptibility to pyogenic bacteria and *Mycobacterium* infection. Every patient had a mutation in the *NEMO* gene that caused reduced NF-κB activation in a NEMO reconstitution assay, as described in "Proliferation of $NEMO^{normal}$ and $NEMO^{low}$ T cells." Patient profiles are listed in Table 1.

Flow cytometric analysis

NEMO intracellular staining was performed as previously described.[17] The cells were stained for the following lineage markers before staining for NEMO: CD4, CD8, CD14, CD15, CD19, CD56, CD45RA (BD Biosciences/BD Pharmingen), and CCR7 (R&D Systems Inc). Intracellular staining of human IFN-γ, TNF-α, and NEMO was performed as previously described.[18] The stained cells were collected using a FACSCalibur flow cytometer (BD Biosciences) and analyzed using the FlowJo software (TreeStar).

Reporter assay

Wild-type and mutant *NEMO* cDNAs were generated from a healthy volunteer and the recruited XL-EDA-ID patients by RT-PCR; the cDNAs were subcloned into the p3xFLAG-CMV14 vector (Sigma-Aldrich). NEMO null rat fibroblast cells (kindly provided by Dr S. Yamaoka, Department of Molecular Virology, Graduate School of Medicine, Tokyo Medical and Dental University, Tokyo, Japan) were plated at a density of

3×10^4 cells/well in a 24-well culture dish and were transfected with 40 ng of NF-κB reporter plasmid (pNF-κB-Luc; BD Biosciences/BD Clontech), 2 ng of *NEMO* mutant expression construct, 10 ng of internal control for the normalization of transfection efficiency (pRL-TK; Toyo Ink), and 148 ng of mock vector using FuGENE HD Transfection Reagent (TOYO-B-Net) according to the manufacturer's protocol. Twelve hours after transfection, the cells were stimulated with 15 ng/mL lipopolysaccharide (LPS; Sigma-Aldrich) for 4 hours and the NF-κB activity was measured using the PicaGene Dual SeaPansy assay kit (TOYO-B-Net). Experiments were performed in triplicate and firefly luciferase activity was normalized to *Renilla* luciferase activity.

Subcloning analysis of cDNA

Cell sorting of the various cell lineages was performed by FACSVantage (BD Biosciences). The purity of each lineage was > 95%. The cDNA from sorted cells was purified and reverse transcribed by Super Script III (Invitrogen) with random hexamers and amplified by the proofreading PCR enzyme KOD, as previously described.[17,21] The PCR primers used were NEMO2 (5′-AGAGACGAAGGAGCACAAAGCTGCCTTGAG-3′) and NEMO3 (5′-ACTGCAGGGACAATGGTGGGTGCATCTGTC-3′). The PCR products were subcloned using a TA cloning kit (Invitrogen) and sequenced by ABI 3130xl Genetic analyzer (Applied Biosystems). To determine whether additional mutations occurred in revertant subclones that had wild-type sequence in the original mutation site, the entire coding region of the *NEMO* gene was sequenced and an additional mutation was considered present when the same mutation was detected in multiple subclones.

Allele-specific PCR

The mRNA purified from sorted T cells and monocytes was reverse-transcribed by SuperScript III (Invitrogen) with the gene-specific primer NEMO2 and amplified by the proofreading PCR enzyme KOD (Toyobo) using the primers NEMO3 and NEMO 4 (5′-TGTGGACACGCAGTGAAACGTGGTCTGGAG-3′). The PCR products were used as templates for allele-specific PCRs with Ex Taq polymerase (Takara Bio). Mutant and wild-type *NEMO* DNA was generated from each NEMO expression plasmid, mixed at graded ratios, and used as controls. PCR conditions and primer sequences are listed in supplemental Table 1 (available on the *Blood* Web site; see the Supplemental Materials link at the top of the online article).

Proliferation of NEMO^{normal} and NEMO^{low} T cells

To obtain PHA-induced T-cell blasts, PBMCs were stimulated with PHA (1:100; Invitrogen) and cultured in RPMI 1640 supplemented with 5% FCS and recombinant human IL-2 (50 IU/mL; kindly provided by Takeda Pharmaceutical Company) at 37°C for 7 days. Subcloning analysis of the cDNA obtained from the T-cell blasts was performed as described in "Subcloning analysis of cDNA."

Results

Reversion mosaicism of NEMO occurred in siblings with similar immunologic phenotypes

We previously reported patient 1 with a duplication mutation of the *NEMO* gene spanning intron 3 to exon 6, who was diagnosed as XL-EDA-ID at 1 year of age after suffering from recurrent infections.[17] At first, genetic diagnosis of the patient was difficult because the expression of aberrant *NEMO* mRNA was masked by the expression of normal *NEMO* mRNA by the revertant cells. Flow cytometric analysis of intracellular NEMO expression revealed cells with normal (NEMO^{normal}) and reduced (NEMO^{low}) levels of NEMO expression, indicating the presence of reversion mosaicism of the *NEMO* gene, and further analysis revealed that the *NEMO* mutation was disease-causing. PCR across the mutated region and sequencing of the PCR products revealed a duplication extending from intron 3 to exon 6, which was confirmed by Southern blot analysis. Additional copy number analysis of the *NEMO* gene of patient 1 and his mother excluded the possibility of a complex chromosomal aberration such as multiple duplication of the *NEMO* gene (supplemental Figure 1). Furthermore, polymorphism analysis using variable number tandem repeats on NEMO^{normal} and NEMO^{low} cells from patient 1 revealed that these cells were derived from the same origin (supplemental Table 2), indicating that the *NEMO* gene mosaicism was less likely because of amalgamation. The genomic analysis of the NEMO^{normal} cells revealed a complete reversion of the *NEMO* gene with no additional mutations. The clinical phenotype of patient 1 was combined immunodeficiency with a reduced number of T cells and mitogen-induced proliferation (Tables 2-3). We previously determined that reduced NEMO expression in the mutant T cells caused impairment of T-cell development and mitogen-induced proliferation.

Patient 2, the younger brother of patient 1, was diagnosed as XL-EDA-ID with the same duplication mutation as his brother. Flow cytometric analysis of intracellular NEMO expression performed at diagnosis showed that most of his PBMCs had reduced NEMO expression (Figure 1A). At 2 months of age, when most of the T cells were NEMO^{low}, absolute counts of the patient's T cells and the mitogen-induced proliferation of the patient's PBMCs were comparable with those of the healthy controls (Figure 1A-B; Table 2). These findings indicated that the *NEMO* mutation had no effect on T-cell development and mitogen-induced proliferation during early infancy in patient 2.

NEMO^{normal} T cells gradually increased as patient 2 grew older, while the absolute count of NEMO^{low} T cells decreased (Figure 1A-B). Accordingly, normal full-length *NEMO* cDNA, which had been undetectable in cord blood, was detectable in the patient's peripheral blood at 12 months of age. However, while NEMO^{normal} T cells were increasing, mitogen-induced T-cell proliferation started to decrease (Table 3), and the patient started to show poor weight gain from 6 months of age. When patient 2 was 17 months old, a blood culture revealed an *M szulgai* bacteremia. At this time, the absolute count of NEMO^{normal} T cells peaked, and NEMO^{low} T cells were at a minimum. He began to gain weight after anti-*Mycobacterium* medication was initiated, although NEMO^{normal} T cells started to decrease and NEMO^{low} T cells began to increase (Figure 1B). When the patient was 23 months old, mitogen-induced T-cell proliferation was still low and a roughly equal number of NEMO^{low} and NEMO^{normal} T cells were detected (Table 3). Overall, as patient 2 grew older, NEMO^{normal} T cells increased as the total number of T cells and the mitogen-induced T-cell proliferation decreased, similar to what had occurred in patient 1 at a similar age.

Various analyses were performed to compare the immunologic phenotype of NEMO^{low} and NEMO^{normal} T cells in detail. Both NEMO^{normal} and NEMO^{low} CD4$^+$ T cells carried a diverse Vβ repertoire, but CD8$^+$ T cells had a skewed Vβ repertoire regardless of NEMO expression level (Figure 1C). Surface marker analysis revealed that most of the NEMO^{normal} T cells were CD45RA$^-$/CCR7$^-$ and most of the NEMO^{low} T cells were CD45RA$^+$/CCR7$^+$ (Figure 1D). The NEMO^{normal} T cells produced similar amounts of IFN-γ and TNF-α as healthy control cells, while the production of these cytokines were reduced in NEMO^{low} T cells (Figure 1E-F). Taken together, these data implied that the immunologic phenotype of T cells from patient 2 converged with that of patient 1 as patient 2 grew older.

Table 2. Surface marker analysis of peripheral mononuclear cells of patients 1 and 2

	Patient 1	Patient 2		Healthy controls
Age at analysis	2 y	2 mo	19 mo	
CD3	1503	2366	1014	2997 ± 1751
CD4	292	1583	374	1683 ± 874
CD8	1160	783	547	1114 ± 976
TCRαβ	1386	2295	439	2620 ± 1612
TCRγδ	109	74	574	343 ± 177
CD4+CD45RA	58	1336	105	1471 ± 890
CD4+CD45RO	263	307	266	497 ± 189
CD8+CD45RA	1178	783	297	1083 ± 1078
CD8+CD45RO	361	21	250	385 ± 442
CD4+CD25	80	427	93	210 ± 99
CD19	1200	941	1543	1252 ± 1145
CD20	1189	931	1536	1125 ± 837
CD19+Sm-IgG	7	18	17	54 ± 21
CD19+Sm-IgA	15	4	14	18 ± 14
CD19+Sm-IgM	1171	910	1505	1057 ± 881
CD19+Sm-IgD	1171	906	1495	1052 ± 884
CD16	912	176	24	287 ± 200
CD56	908	176	24	306 ± 207

Surface markers expressed by XL-EDA-ID patients' PBMCs are shown as absolute counts per microliter of peripheral blood. Healthy control values are based on children aged 1 to 6 years and are shown as the mean ± SD.

Sm indicates the surface membrane.

High incidence of somatic mosaicism of the *NEMO* gene in XL-EDA-ID patients

It is worth noting that somatic reversion mosaicism of the *NEMO* gene occurred in both of the 2 XL-EDA-ID siblings carrying a duplication mutation. To determine whether a high frequency of reversion is a specific event for this type of *NEMO* duplication mutation[22-25] or if the reversion of the *NEMO* gene occurs commonly in XL-EDA-ID patients, we recruited an additional 8 XL-EDA-ID patients from throughout Japan (Table 1) and analyzed the presence of *NEMO* reversion. These patients had various combinations of clinical phenotypes characteristic of XL-EDA-ID such as ectodermal dysplasia, innate and acquired immunity defects, and susceptibility to pyogenic bacteria and *Mycobacterium* infections. Every patient had a mutation of the *NEMO* gene with reduced NF-κB activation potential, as evaluated in a NEMO reconstitution assay (Figure 2).

Among the 8 patients, only patient 3 had a large proportion of NEMO^{low} cells by flow cytometric analysis. The majority of patient 3's PBMCs were NEMO^{low}, whereas 10% of the patient's CD8$^+$ cells were NEMO^{normal} (Figure 3A). This patient was identified as carrying the D311E mutation. Because missense mutations of the *NEMO* gene often do not result in the reduced expression of NEMO protein, subcloning and sequencing analysis was performed on the *NEMO* cDNA isolated from the remaining patients, and 6 of the 7 patients had normal *NEMO* subclones (Table 3). Expansion of maternal cells after fetomaternal transfusion was ruled out in these patients by FISH analysis with X and Y probes (Table 1).

Additional genetic analysis of the entire coding region of the *NEMO* gene was performed on NEMO^{normal} cells from patient 3 and on reverted subclones from the other patients, except for patient 10 who had already received stem cell transplantation. The *NEMO* gene in these samples had reverted to wild-type with no additional mutations (Figure 3B and data not shown). To specifically determine in which cell lineages the reversion occurred, subcloning and sequencing analysis of cDNA in various cell lineages was performed. This analysis revealed that all the revertant cells were of the T-cell lineage and that no reversion occurred in monocytes and very little occurred in B cells (Table 4). Allele-specific PCR confirmed that reversion occurred in T cells but not in monocytes (Figure 4).

Selective advantage of NEMO^{normal} cells in XL-EDA-ID carriers

The high frequency of somatic mosaicism in T cells of XL-EDA-ID patients indicated a strong selective advantage of wild-type NEMO T cells over T cells carrying mutant NEMO. To confirm this hypothesis, *NEMO* cDNA analysis was performed on various cell lineages from the mothers of the patients who are heterozygous for *NEMO* mutation and thus have mosaicism

Table 3. Immunologic analysis of patients 1 and 2

	Patient 1	Patient 2 (treated with IVIG)	
Age at analysis, mo	9	9	20
Serum immunoglobulin levels, g/L (control)			
IgG	10.63 (4.51-10.46)	8.44 (4.51-10.46)	10.37 (7.15-9.07)
IgA	1.36 (0.14-0.64)	1.88 (0.14-0.64)	3.93 (0.22-1.44)
IgM	0.4 (0.33-1.00)	0.17 (0.33-1.00)	0.20 (0.34-1.28)
Age at analysis	2 y	2 mo	23 mo
T-cell proliferation, SI (control)	9.3 (206.9 ± 142.5)	55.3 (64.8 ± 8.1)	7.2 (89.4 ± 31.2)

Control values of serum immunoglobulin levels are based on children aged either 7 to 9 months or 1 to 2 years and are shown as the mean ± SD. The T-cell proliferation assay was performed as described previously[17] with at least three healthy adults as controls.

SI indicates stimulation index; and IVIG, 2.5 g of monthly IV immune globulin infusion.

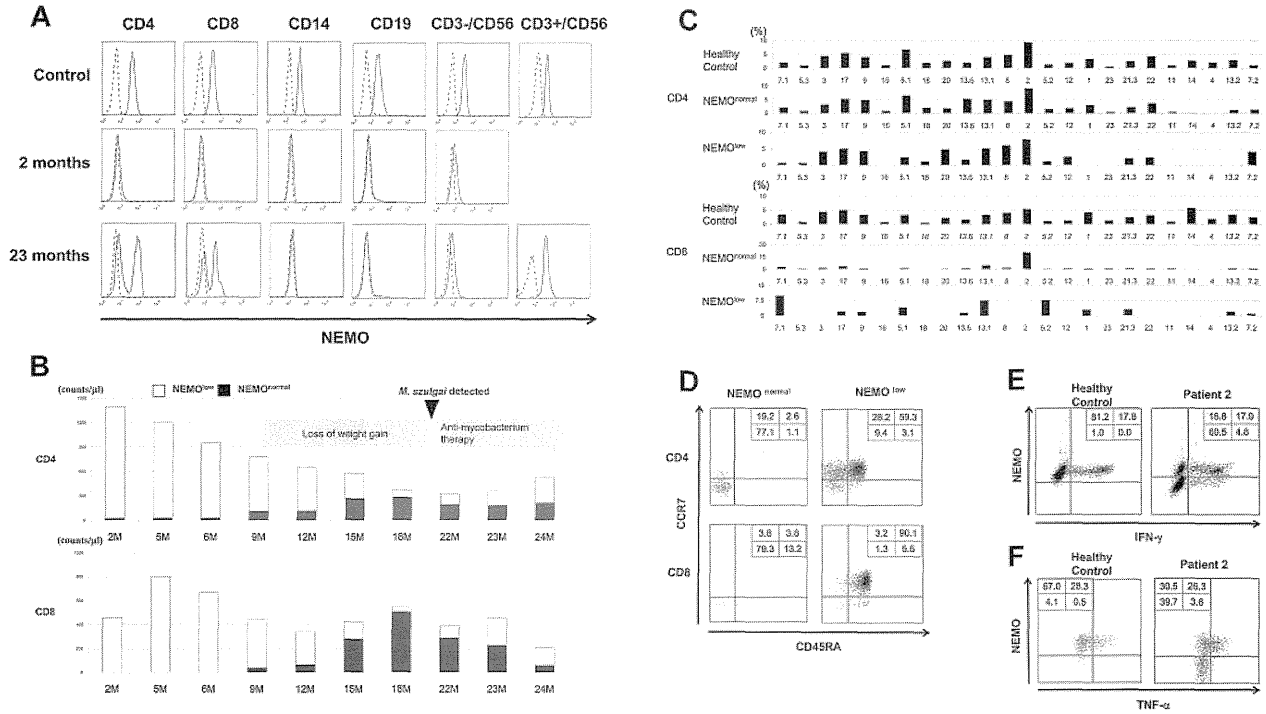

Figure 1. Identification and characterization of *NEMO* revertant T cells in patient 2. (A) Intracellular expression of NEMO in various PBMC lineages from a healthy adult control and patient 2 were evaluated by flow cytometry. For the patient, results of the analyses performed at 2 months and 23 months are shown. Solid lines indicate staining with the anti-NEMO mAb, and dotted lines indicate the isotype control. (B) Time-course variations in the absolute count of $NEMO^{normal}$ and $NEMO^{low}$ T cells in patient 2. M indicates age in months. (C) TCR-Vβ repertoire analysis of the patient's $CD4^+$ and $CD8^+$ T cells. PBMCs from the patient and a healthy adult control were stained for the TCR-Vβ panel, CD4, CD8, and NEMO, and analyzed by flow cytometry. (D) Phenotype analysis of T cells in patient 2. PBMCs from the patient and a control were stained for the expression of NEMO, CCR7, CD45RA, and CD4 or CD8. Data shown were gated on $NEMO^{normal}$ or $NEMO^{low}$ $CD4^+$ or $CD8^+$ cells. (E-F) Cytokine production from $NEMO^{normal}$ and $NEMO^{low}$ T cells. PBMCs from the patient and a control were stimulated with PMA and ionomycin for 6 hours and stained for intracellular (E) IFN-γ or (F) TNF-α along with NEMO. Cells shown are gated on the $CD3^+$ population.

because of X-chromosome inactivation. This analysis assumes that the percentage of cDNA for wild-type *NEMO* reflects the percentage of cells expressing wild-type NEMO. A high proportion of wild-type *NEMO* cDNA was observed in T cells from the mothers of patients 1/2, 3, 8, and 10, although wild-type *NEMO* cDNA was not predominant in T cells from the mother of patient 4 (Table 5).

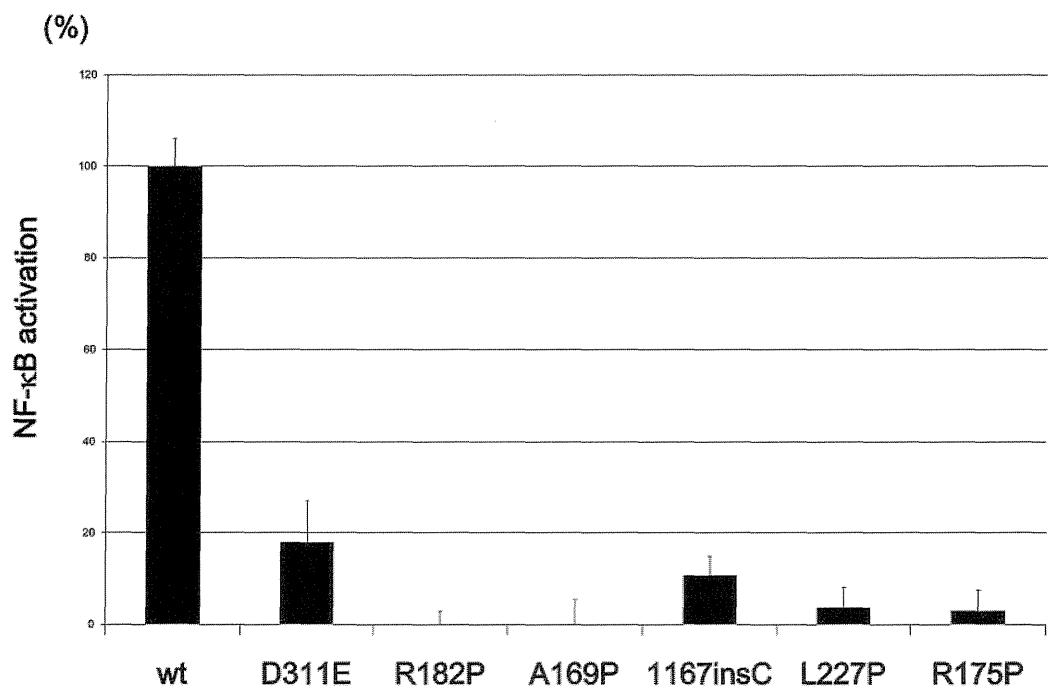

Figure 2. NF-κB transactivation by NEMO mutants from the XL-EDA-ID patients. NF-κB transactivation induced by NEMO mutants in the XL-EDA-ID patients. Mock vectors and wild-type (wt) NEMO were used as controls. The NF-κB activation index of NEMO variants were calculated as (NF-κB activation by each NEMO variant − NF-κB activation of the mock vector)/(NF-κB activation by wild-type NEMO − NF-κB activation of the mock vector). The data shown are the mean ± SD of triplicate wells and are representative of 3 independent experiments with similar results.

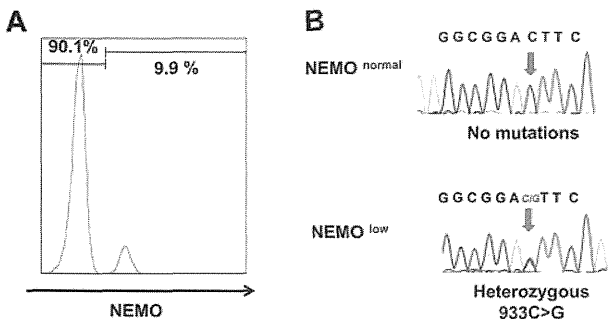

Figure 3. *NEMO* revertant T cells in patient 3. (A) Intracellular expression of NEMO in $CD8^+$ cells from patient 3. (B) Sequencing chromatograms of DNA from $NEMO^{normal}$ or $NEMO^{low}$ $CD8^+$ cells of patient 3. Arrows indicate the mutated base position at c. 931.

Similarly, there was an apparent high proportion of wild-type *NEMO* cDNA in monocytes and B cells from the mothers of patients 1/2, 8, and 10 (Table 5). These findings suggested a general selective advantage of $NEMO^{normal}$ cells over $NEMO^{low}$ cells in vivo, especially in T cells.

Proliferation capacity of $NEMO^{normal}$ and $NEMO^{low}$ T cells

T-cell proliferation stimulated by mitogens such as PHA is usually not reduced in XL-EDA-ID patients. However, the emergence of $NEMO^{normal}$ cells coincided with a reduction in mitogen-induced proliferation in patient 2. To further determine the effect of $NEMO^{normal}$ cells on mitogen-induced proliferation of peripheral T cells, the proportions of T cells carrying the wild-type and mutant were examined before and after PHA stimulation in XL-EDA-ID patients and their mothers (Table 6). In patients 2, 4, and 8, the percentage of the $NEMO^{normal}$ cells decreased after PHA stimulation, while $NEMO^{normal}$ cells prevailed in patient 9. In the mothers of patient 4 and 10, the percentage of $NEMO^{normal}$ cells increased after PHA stimulation, while the percentage of the $NEMO^{normal}$ cells decreased in the mother of patient 3. These results indicated that the NEMO mutation does not directly affect the mitogen-induced proliferation capacity of T cells and factors other than the *NEMO* genotype determine the proliferation capacity of $NEMO^{normal}$ and $NEMO^{low}$ T cells.

Discussion

Somatic reversion mosaicism has been described in several disorders affecting the hematopoietic system, the liver, and the skin.[23,26] Reports of somatic reversion cases have been particularly abundant in patients with immunodeficiency diseases, including Wiskott-Aldrich syndrome (WAS)[27] and SCID, which occur because of mutations in the interleukin receptor common γ chain,[28] CD3ζ,[29] *RAG-1*[30], and *ADA* genes.[31] Patients with somatic reversion mosaicism may present with significantly milder clinical phenotypes compared with nonrevertant patients with the same germline mutation, although this is not always the case.[26] One common feature in most cases where the somatic reversion mosaicism has been observed is a strong in vivo selective advantage of the revertant cells that express the wild-type gene product. One of the most intensively investigated diseases associated with somatic reversion mosaicism is WAS.[32-34] A report showed that up to 11% of WAS patients have presented with somatic reversion mosaicism.[33]

In our investigation, 9 of 10 XL-EDA-ID patients presented with somatic mosaicism. Two of the 9 were cases of reversion from a duplication mutation, while the others exhibited true back-reversion from a substitution or insertion mutation. This finding calls for caution when diagnosing XL-EDA-ID patients. Because the existence of a *NEMO* pseudogene makes it difficult to perform genetic analysis using genomic DNA, diagnosis of the disease is often confirmed by sequencing analysis of *NEMO* cDNA, and the presence of somatic mosaicism can cause misdiagnosis of XL-EDA-ID patients either when $NEMO^{normal}$ cells make up the majority of the patients' PBMCs or when the cDNA of the mutated *NEMO* gene cannot be amplified by PCR.[17] In fact, mutated *NEMO* cDNA could not be amplified from the PBMCs of patient 2 even when $NEMO^{normal}$ cells were absent (during early infancy), and only wild-type *NEMO* cDNA was amplified after the appearance of $NEMO^{normal}$ cells (data not shown), probably because of the instability of the mutated *NEMO* mRNA. Flow cytometric analysis of intracellular NEMO protein is of help in identifying the $NEMO^{low}$ cells in some patients, but the technique is not applicable when the *NEMO* mutation does not cause reduced expression of NEMO protein. Thus, some cases of XL-EDA-ID patients with reversion may be difficult to diagnose.

The high frequency of somatic mosaicism observed in XL-EDA-ID patients indicates a strong in vivo selective advantage for $NEMO^{normal}$ cells, which express the wild-type gene product. Patient 2 presented with a high mutant T-cell count at birth that gradually decreased over time (Figure 1B). This finding indicates that wild-type NEMO expression is critical for the survival of certain cell lineages, including T cells, after birth. On the other hand, no $NEMO^{normal}$ monocytes and very few $NEMO^{normal}$ B cells were detected in the recruited XL-EDA-ID patients (Table 4). This specific feature is similar to other somatic reversion mosaicism seen in primary immunodeficiency patients[26] and indicates that the expression of NEMO is less critical for the survival of monocytes or B cells compared with that of T cells. There is also an apparent

Table 4. Analysis of *NEMO* gene mosaicism in various cell lineages for each patient

Patient	Mutation	Age at analysis	CD4, % (proportion)	CD8, % (proportion)	CD14, % (proportion)	CD19, % (proportion)
1	Duplication	2 y	90	100	0	4.0
2	Duplication	15 mo	45	66	0	4.0
3	D311E	3 y	2.4	9.9	0	1.2
4	A169P	12 y	0 (0/19)	24 (9/37)	0 (0/19)	0 (0/47)
5	L227P	3 y	0 (0/25)	0 (0/35)	0 (0/30)	0 (0/25)
6	R182P	4 y	18 (5/28)	17 (9/52)	0 (0/27)	0 (0/33)
7	R175P	6 y	0.4 (1/25)	39 (11/28)	0 (0/28)	0 (0/25)
8	Q348X	8 y	38 (6/16)	47 (9/19)	0 (0/33)	0 (0/25)
9	R175P	15 y	30 (9/30)	36 (12/33)	0 (0/23)	0 (0/14)
10	1167 ins C	9 mo		PBMC 9.3 (4/43)		

For patients 1 to 3, data represent the percentages of $NEMO^{normal}$ cells in each lineage, as assessed by flow cytometry. For patients 4 to 10, the ratio indicates the number of wild-type NEMO clones in various cell lineages as compared with the total number of clones analyzed, based on subcloning and sequencing analysis.

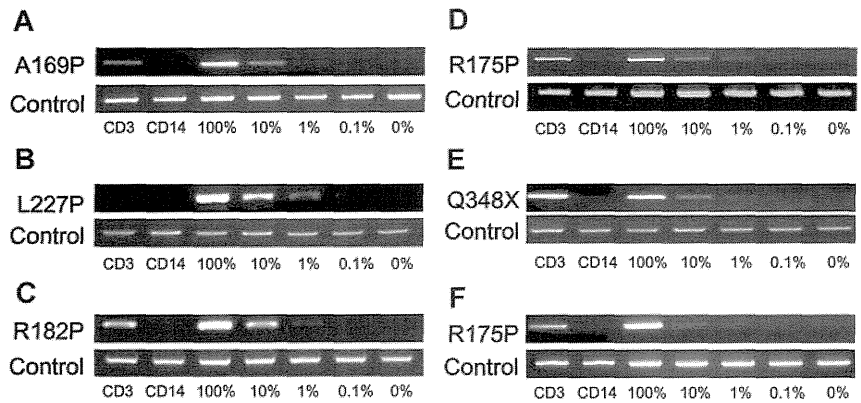

Figure 4. NEMO reversion selectively occurs in T cells of XL-EDA-ID patients. Allele-specific PCR for *NEMO* on $CD3^+$ or $CD14^+$ cells from (A) patient 4, (B) patient 5, (C) patient 6, (D) patient 7, (E) patient 8, and (F) patient 9. Numbers below each figure indicate the percentages of wild-type NEMO cDNA mixed with each mutant. Primers used in each PCR are shown on the left.

concordance between the degree of the disruption of *NEMO* gene and the proportion of reverted $NEMO^{normal}$ cells compared with $NEMO^{low}$ cells. The high proportion of reverted T cells seen in patients 1 and 2 as well as in patient 8 was associated with a highly disruptive mutation of the *NEMO* gene (ie, a duplication mutation in patients 1 and 2, and a truncation mutation in patient 8). In addition, the highly selective X-chromosome inactivation observed in the mothers of XL-EDA-ID patients indicated a strong selective advantage for $NEMO^{normal}$ cells over $NEMO^{low}$ cells. It is also noteworthy that reverted T cells were not detected in patient 5, who carried an L227P mutation that was not localized to either of the functional domains in the NEMO protein. Other reported cases with the same mutation presented with polysaccharide-specific humoral immunodeficiency and autoinflammatory diseases, but were spared complications such as cellular immunodeficiency and susceptibility to *Mycobacterium* (similar to patient 5).[4,8] This may reflect the fact that the L227P mutation in NEMO has less influence on T-cell growth than NEMO mutations that occur in functional domains, and suggests that reversion of the mutation has little impact on T-cell survival. Although the number of cases in our study is limited, it appears that the more disruptive NEMO mutations favor the survival of $NEMO^{normal}$ cells after reversion and X-chromosome inactivation.

Regarding the gradual decline in the number of NEMO-deficient T cells, one candidate trigger could be infection. Because the dominance of the memory phenotype and the skewed TCR repertoire among $CD8^+$ T cells in $NEMO^{normal}$ cells were observed in both patients 1 and 2 (Figure 1C and Mizukami et al[18]), continuous infection of pyogenic bacteria in patient 1 and *M szulgai* in patient 2 could be a reason for the emergence of $NEMO^{normal}$ cells and the elimination of $NEMO^{low}$ cells. The decrease in $NEMO^{normal}$ cells and restoration of $NEMO^{low}$ cells after anti-mycobacterial therapy in patient 2 support this hypothesis. In the case of patient 1, the predominance of $NEMO^{normal}$ T cells with an effector/memory phenotype at diagnosis (Table 4 and Mizukami et al[18]) is likely to be the result of chronic infection, and it is possible that $NEMO^{low}$ cells were predominant during his early infancy. Because some reports have indicated that TNF-α–induced programmed cell death of several cell types, including a human T-cell line, was enhanced by hypomorphic *NEMO* mutations,[12,35] and considering our finding that the levels of TNF-α expressed in revertant T cells were similar to levels in healthy control T cells in vitro (Figure 1F), TNF-α produced from these cells in response to infection could be involved in mutant T-cell elimination.

Unexpectedly, T-cell proliferation in patient 2 was equivalent to that of normal controls at the age of 2 months and was reduced after $NEMO^{normal}$ T cells increased (Figure 1B; Table 3). This finding indicates that the $NEMO^{low}$ T cells did not have intrinsically impaired mitogen-induced proliferation. One reasonable explanation for the reduced proliferation observed after the increase in $NEMO^{normal}$ T cells is a reduction in the absolute number of T cells (naive T cells in particular), probably because of the infection.

Table 5. Expression of mutant NEMO in various cell lineages for the mother of each XL-EDA-ID patient

Sample	Mutation	Analysis	Subtype	Mutant type, % (proportion)
Mother of patients 1 and 2	Duplication	FACS	CD3	0
			CD14	0
			CD19	0
Mother of patient 3	D311E	FACS	CD3	13
			$CD3^-$	54
		Subcloning	CD3	22 (6/27)
			$CD3^-$	55 (12/22)
Mother of patient 4	A169P	Subcloning	CD3	52 (11/21)
			CD14	58 (11/19)
			CD19	42 (5/12)
Mother of patient 8	Q348X	Subcloning	CD3	0 (0/26)
			CD14	17 (3/18)
			CD19	0 (0/18)
Mother of patient 10	1167insC	Subcloning	CD3	18 (7/39)
			CD14	12 (5/43)
			CD19	27 (12/44)

Data are shown as either the percentages of $NEMO^{normal}$ cells, as assessed by flow cytometry, or as the ratio of clones containing wild-type NEMO to the total number of clones, as analyzed by subcloning and sequencing analysis.

Table 6. Expression of mutant NEMO in CD3-positive cells and PHA blasts

Sample	Mutations	Analysis	Subtype	Mutant type, % (proportion)
Mother of patient 3	D311E	FACS	CD3	13
			PHA blast	47
		Subcloning	CD3	22 (6/27)
			PHA blast	48 (11/23)
Mother of patient 4	A169P	Subcloning	CD3	52 (11/21)
			PHA blast	18 (9/49)
Mother of patient 8	Q348X	Subcloning	CD3	0 (0/26)
			PHA blast	0 (0/21)
Mother of patient 10	1167insC	Subcloning	CD3	18 (7/39)
			PHA blast	9 (4/43)
Patient 2	Duplication	FACS	CD3	73
			PHA blast	93
Patient 4	A169P	Subcloning	CD3	79 (19/24)
			PHA blast	100 (37/37)
Patient 8	Q348X	Subcloning	CD3	56 (18/32)
			PHA blast	100 (16/16)
Patient 9	R175P	Subcloning	CD3	87 (34/39)
			PHA blast	0 (0/28)

PHA blasts were obtained by incubating PBMCs with PHA and soluble IL-2 for 7 days. Data are shown as either the percentages of $NEMO^{normal}$ cells, as assessed by flow cytometry, or as the ratio of clones containing wild-type NEMO to the total number of clones, as analyzed by subcloning and sequencing analysis.

Therefore, to identify other mechanisms underlying reduced T-cell proliferation, the impact of *NEMO* mutation on PHA-induced T-cell proliferation was indirectly examined in vitro by comparing the response of $NEMO^{normal}$ and $NEMO^{low}$ cells derived from XL-EDA-ID patients and their mothers. After PHA stimulation and proliferation, the proportion of $NEMO^{low}$ T cells increased in patients 2, 4, and 8, while the opposite result was observed in patient 9 and in the mother of patient 4 (Table 6). Although the precise mechanism is unclear, a reduction in the proportion of $NEMO^{normal}$ cells after PHA stimulation would reflect the lower proliferative capacity of $NEMO^{normal}$ cells compared with that of $NEMO^{low}$ cells, which may be another explanation for the reduced T-cell proliferation observed in patient 2 at 23 months of age when $NEMO^{normal}$ T cells were dominant. In the reports on reversion mosaicism of *IL2RG* gene mutations,[28,36] the restoration of T-cell function and clinical symptoms varied among patients. Therefore, other factors besides the genotype of the mutations, such as the developmental stage where reversion occurred and the frequency of reversion, affect the clinical impact of somatic mosaicism of *NEMO* gene mutations.

In this study, the effect of somatic mosaicism of the *NEMO* gene on clinical phenotype could not be fully evaluated. However, cytokines produced by revertant T cells could influence the development of clinical symptoms of XL-EDA-ID, such as inflammatory bowel disease. In a mouse model, intestinal epithelial cell-specific inhibition of NF-κB through the conditional ablation of NEMO resulted in the development of chronic bowel inflammation sensitized intestinal epithelial cells to TNF-α–induced apoptosis.[37] In this model, the first phase of intestinal inflammation was initiated by epithelial cell death and was followed by a second phase of TNF-α–induced intestinal inflammation, the latter being dependent on T cells. Another report showed that HSCT in XL-EDA-ID patients exacerbated the patients' inflammatory bowel disease.[38] Indeed, in patient 4, the percentage of reverted T cells was reduced after repeated administrations of anti-TNFα blocking Ab, and the symptoms of inflammatory bowel disease improved.[18] Considering this evidence, somatic mosaicism in T cells might be an important factor leading to inflammatory disease in XL-EDA-ID patients with defective NF-κB activation. However, our study did not show a tight association between inflammatory bowel disease and somatic mosaicism, and further investigation is needed to determine whether the $NEMO^{normal}$ T cells play a role in inflammatory processes in XL-EDA-ID.

In conclusion, this study has identified a high frequency of somatic mosaicism in XL-EDA-ID patients, particularly in T cells, and has revealed important insights into human T-cell immunobiology in XL-EDA-ID. Although we could not demonstrate the clinical impact of somatic mosaicism in XL-EDA-ID patients, our findings suggest that care is required when making molecular diagnoses of XL-EDA-ID, and might shed light on the mechanisms underlying the variability in the clinical manifestation of XL-ED-ID and facilitate the search for appropriate treatments.

Acknowledgments

The authors are grateful to all the XL-EDA-ID patients and their families for their participation. They also thank Shoji Yamaoka (Department of Molecular Virology, Graduate School of Medicine, Tokyo Medical and Dental University, Tokyo, Japan) for kindly providing NEMO-null rat fibroblast cells, and Takeda Pharmaceutical Company Limited for kindly providing the recombinant human IL-2.

This work was supported by grants from the Japanese Ministry of Education, Culture, Sports, Science, and Technology, and by grants from the Japanese Ministry of Health, Labor and Welfare.

Authorship

Contribution: Tomoki Kawai wrote the manuscript and performed research; R.N., T.Y., T.N., and T.H. edited the manuscript and supervised this work; K.I., Y.M., N.T., H.S., M.S., and Y.T. cultured cells; and T. Mizukami, H.N., Y.K., A.Y., T. Murata, S.S., E.I., H.A., Toshinao Kawai, C.I., S.O., and M.K. treated patients and analyzed data.

Conflict-of-interest disclosure: The authors declare no competing financial interests.

Correspondence: Ryuta Nishikomori, MD, PhD, Department of Pediatrics, Kyoto University Graduate School of Medicine, 54 Kawahara-cho, Shogoin, Sakyo-ku, Kyoto 606-8507, Japan; e-mail: rnishiko@kuhp.kyoto-u.ac.jp.

References

1. Pinheiro M, Freire-Maia N. Ectodermal dysplasias: a clinical classification and a causal review. *Am J Med Genet.* 1994;53(2):153-162.
2. Abinun M, Spickett G, Appleton AL, Flood T, Cant AJ. Anhidrotic ectodermal dysplasia associated with specific antibody deficiency. *Eur J Pediatr.* 1996;155(2):146-147.
3. Sitton JE, Reimund EL. Extramedullary hematopoiesis of the cranial dura and anhidrotic ectodermal dysplasia. *Neuropediatrics.* 1992;23(2):108-110.
4. Schweizer P, Kalhoff H, Horneff G, Wahn V, Diekmann L. [Polysaccharide specific humoral immunodeficiency in ectodermal dysplasia. Case report of a boy with two affected brothers]. *Klin Padiatr.* 1999;211(6):459-461.
5. Abinun M. Ectodermal dysplasia and immunodeficiency. *Arch Dis Child.* 1995;73(2):185.
6. Zonana J, Elder ME, Schneider LC, et al. A novel X-linked disorder of immune deficiency and hypohidrotic ectodermal dysplasia is allelic to incontinentia pigmenti and due to mutations in IKK-gamma (NEMO). *Am J Hum Genet.* 2000;67(6):1555-1562.
7. Courtois G, Smahi A, Israel A. NEMO/IKK gamma: linking NF-kappa B to human disease. *Trends Mol Med.* 2001;7(10):427-430.
8. Doffinger R, Smahi A, Bessia C, et al. X-linked anhidrotic ectodermal dysplasia with immunodeficiency is caused by impaired NF-kappaB signaling. *Nat Genet.* 2001;27(3):277-285.
9. Rothwarf DM, Zandi E, Natoli G, Karin M. IKK-gamma is an essential regulatory subunit of the IkappaB kinase complex. *Nature.* 1998;395(6699):297-300.
10. Yamaoka S, Courtois G, Bessia C, et al. Complementation cloning of NEMO, a component of the IkappaB kinase complex essential for NF-kappaB activation. *Cell.* 1998;93(7):1231-1240.
11. Smahi A, Courtois G, Vabres P, et al. Genomic rearrangement in NEMO impairs NF-kappaB activation and is a cause of incontinentia pigmenti. The International Incontinentia Pigmenti (IP) Consortium. *Nature.* 2000;405(6785):466-472.
12. Hanson EP, Monaco-Shawver L, Solt LA, et al. Hypomorphic nuclear factor-kappaB essential modulator mutation database and reconstitution system identifies phenotypic and immunologic diversity. *J Allergy Clin Immunol.* 2008;122(6):1169-1177.
13. Orange JS, Jain A, Ballas ZK, Schneider LC, Geha RS, Bonilla FA. The presentation and natural history of immunodeficiency caused by nuclear factor kappaB essential modulator mutation. *J Allergy Clin Immunol.* 2004;113(4):725-733.
14. Jain A, Ma CA, Liu S, Brown M, Cohen J, Strober W. Specific missense mutations in NEMO result in hyper-IgM syndrome with hypohydrotic ectodermal dysplasia. *Nat Immunol.* 2001;2(3):223-228.
15. Orange JS, Brodeur SR, Jain A, et al. Deficient natural killer cell cytotoxicity in patients with IKK-gamma/NEMO mutations. *J Clin Invest.* 2002;109(11):1501-1509.
16. Sebban H, Courtois G. NF-kappaB and inflammation in genetic disease. *Biochem Pharmacol.* 2006;72(9):1153-1160.
17. Nishikomori R, Akutagawa H, Maruyama K, et al. X-linked ectodermal dysplasia and immunodeficiency caused by reversion mosaicism of NEMO reveals a critical role for NEMO in human T-cell development and/or survival. *Blood.* 2004;103(12):4565-4572.
18. Mizukami T, Obara M, Nishikomori R, et al. Successful treatment with infliximab for inflammatory colitis in a patient with X-linked anhidrotic ectodermal dysplasia with immunodeficiency. *J Clin Immunol.* 2012;32(1):39-49.
19. Imamura M, Kawai T, Okada S, et al. Disseminated BCG infection mimicking metastatic nasopharyngeal carcinoma in an immunodeficient child with a novel hypomorphic NEMO mutation. *J Clin Immunol.* 2011;31(5):802-810.
20. Tono C, Takahashi Y, Terui K, et al. Correction of immunodeficiency associated with NEMO mutation by umbilical cord blood transplantation using a reduced-intensity conditioning regimen. *Bone Marrow Transplant.* 2007;39(12):801-804.
21. Saito M, Nishikomori R, Kambe N, et al. Disease-associated CIAS1 mutations induce monocyte death, revealing low-level mosaicism in mutation-negative cryopyrin-associated periodic syndrome patients. *Blood.* 2008;111(4):2132-2141.
22. Yang TP, Stout JT, Konecki DS, Patel PI, Alford RL, Caskey CT. Spontaneous reversion of novel Lesch-Nyhan mutation by HPRT gene rearrangement. *Somat Cell Mol Genet.* 1988;14(3):293-303.
23. Zhang LH, Jenssen D. Reversion of the hprt mutant clone SP5 by intrachromosomal recombination. *Carcinogenesis.* 1992;13(4):609-615.
24. Monnat RJ Jr, Chiaverotti TA, Hackmann AF, Maresh GA. Molecular structure and genetic stability of human hypoxanthine phosphoribosyltransferase (HPRT) gene duplications. *Genomics.* 1992;13(3):788-796.
25. Rautenstrauss B, Liehr T, Fuchs C, et al. Mosaicism for Charcot-Marie-Tooth disease type 1A: onset in childhood suggests somatic reversion in early developmental stages. *Int J Mol Med.* 1998;1(2):333-337.
26. Wada T, Candotti F. Somatic mosaicism in primary immune deficiencies. *Curr Opin Allergy Clin Immunol.* 2008;8(6):510-514.
27. Ariga T, Kondoh T, Yamaguchi K, et al. Spontaneous in vivo reversion of an inherited mutation in the Wiskott-Aldrich syndrome. *J Immunol.* 2001;166(8):5245-5249.
28. Stephan V, Wahn V, Le Deist F, et al. Atypical X-linked severe combined immunodeficiency due to possible spontaneous reversion of the genetic defect in T cells. *N Engl J Med.* 1996;335(21):1563-1567.
29. Rieux-Laucat F, Hivroz C, Lim A, et al. Inherited and somatic CD3zeta mutations in a patient with T-cell deficiency. *N Engl J Med.* 2006;354(18):1913-1921.
30. Wada T, Toma T, Okamoto H, et al. Oligoclonal expansion of T lymphocytes with multiple second-site mutations leads to Omenn syndrome in a patient with RAG1-deficient severe combined immunodeficiency. *Blood.* 2005;106(6):2099-2101.
31. Hirschhorn R. In vivo reversion to normal of inherited mutations in humans. *J Med Genet.* 2003;40(10):721-728.
32. Wada T, Schurman SH, Jagadeesh GJ, Garabedian EK, Nelson DL, Candotti F. Multiple patients with revertant mosaicism in a single Wiskott-Aldrich syndrome family. *Blood.* 2004;104(5):1270-1272.
33. Stewart DM, Candotti F, Nelson DL. The phenomenon of spontaneous genetic reversions in the Wiskott-Aldrich syndrome: a report of the workshop of the ESID Genetics Working Party at the XIIth Meeting of the European Society for Immunodeficiencies (ESID). Budapest, Hungary October 4-7, 2006. *J Clin Immunol.* 2007;27(6):634-639.
34. Davis BR, Yan Q, Bui JH, et al. Somatic mosaicism in the Wiskott-Aldrich syndrome: molecular and functional characterization of genotypic revertants. *Clin Immunol.* 2010;135(1):72-83.
35. Yamaoka S, Inoue H, Sakurai M, et al. Constitutive activation of NF-kappa B is essential for transformation of rat fibroblasts by the human T-cell leukemia virus type I Tax protein. *EMBO J.* 1996;15(4):873-887.
36. Speckmann C, Pannicke U, Wiech E, et al. Clinical and immunologic consequences of a somatic reversion in a patient with X-linked severe combined immunodeficiency. *Blood.* 2008;112(10):4090-4097.
37. Nenci A, Becker C, Wullaert A, et al. Epithelial NEMO links innate immunity to chronic intestinal inflammation. *Nature.* 2007;446(7135):557-561.
38. Fish JD, Duerst RE, Gelfand EW, Orange JS, Bunin N. Challenges in the use of allogeneic hematopoietic SCT for ectodermal dysplasia with immune deficiency. *Bone Marrow Transplant.* 2009;43(3):217-221.

PLOS ONE

Selective Development of Myogenic Mesenchymal Cells from Human Embryonic and Induced Pluripotent Stem Cells

Tomonari Awaya[1]*, Takeo Kato[1], Yuta Mizuno[1], Hsi Chang[1], Akira Niwa[1,2], Katsutsugu Umeda[1], Tatsutoshi Nakahata[2], Toshio Heike[1]

1 Department of Pediatrics, Kyoto University Graduate School of Medicine, Kyoto, Japan, **2** Center for iPS Cell Research and Application (CiRA), Kyoto University, Kyoto, Japan

Abstract

Human embryonic stem (ES) cells and induced pluripotent stem (iPS) cells are promising sources for the cell therapy of muscle diseases and can serve as powerful experimental tools for skeletal muscle research, provided an effective method to induce skeletal muscle cells is established. However, the current methods for myogenic differentiation from human ES cells are still inefficient for clinical use, while myogenic differentiation from human iPS cells remains to be accomplished. Here, we aimed to establish a practical differentiation method to induce skeletal myogenesis from both human ES and iPS cells. To accomplish this goal, we developed a novel stepwise culture method for the selective expansion of mesenchymal cells from cell aggregations called embryoid bodies. These mesenchymal cells, which were obtained by dissociation and re-cultivation of embryoid bodies, uniformly expressed CD56 and the mesenchymal markers CD73, CD105, CD166, and CD29, and finally differentiated into mature myotubes *in vitro*. Furthermore, these myogenic mesenchymal cells exhibited stable long-term engraftment in injured muscles of immunodeficient mice *in vivo* and were reactivated upon subsequent muscle damage, increasing in number to reconstruct damaged muscles. Our simple differentiation system facilitates further utilization of ES and iPS cells in both developmental and pathological muscle research and in serving as a practical donor source for cell therapy of muscle diseases.

Citation: Awaya T, Kato T, Mizuno Y, Chang H, Niwa A, et al. (2012) Selective Development of Myogenic Mesenchymal Cells from Human Embryonic and Induced Pluripotent Stem Cells. PLoS ONE 7(12): e51638. doi:10.1371/journal.pone.0051638

Editor: Atsushi Asakura, University of Minnesota Medical School, United States of America

Received June 27, 2012; **Accepted** November 2, 2012; **Published** December 7, 2012

Funding: This work was supported by a grant from the Japan Ministry of Education, Culture, Sports, Science and Technology. The funders had no role in study design, data collection and analysis, decision to publish, or preparation of the manuscript.

Competing Interests: The authors have declared that no competing interests exist.

* E-mail: awaya@kuhp.kyoto-u.ac.jp

Introduction

Duchenne muscular dystrophy (DMD) is the most common and well-investigated form of muscular dystrophy inherited in an X-linked recessive manner. The molecular deficits underlying this disorder are primarily involved in muscular structural integrity and result in continuous damage to the muscles due to contraction-induced mechanical stress. This damage leads to the rapid wasting of skeletal muscles and to the early deaths of affected patients [1]. Satellite cells, which are muscle-specific stem cells that reside in the muscle [2], maintain the ability of skeletal muscles to undergo self-repair and can be mobilized for reconstruction when the muscles are damaged from exercise and daily activities [3–5]. Although muscular regeneration occurs at a higher frequency in DMD patients than in non-affected individuals [6], it is insufficient to maintain muscle function throughout life. If satellite cells were able to restore damaged muscles more efficiently, the courses of the diseases might be less severe, as observed in mdx mice, a DMD model that is fertile and has a near-normal lifespan [1,7,8]. Despite extensive efforts to develop pharmacological agents to halt the clinical course of DMD, the disease still results in high mortality in patients during late adolescence.

Cell replacement therapy using extrinsic myogenic cells is one of the most promising treatment modalities for muscular dystrophies. Somatic stem cells with skeletal myogenic potential, such as myoblasts, mesenchymal stem cells, side population cells of muscles and bone marrow, pericytes, and hemangioblasts, are known to reside in various types of adult tissues. These cells regenerate diseased muscles in mdx mice; however, clinical trials involving allogeneic myoblast transplantation in DMD patients have not obtained satisfactory results because of immune rejection, rapid death, and the limited migration of transplanted myoblasts [9–11].

Embryonic stem (ES) cells are totipotent stem cells derived from blastocysts [12,13] and possess considerable advantages over somatic stem cells. Because ES cells have theoretically unlimited proliferative capacity, they could be a reliable cell source for regeneration therapy, provided that an effective myogenic differentiation protocol is established. Moreover, recently established induced pluripotent stem (iPS) cells have also become an attractive option for regeneration therapy because they possess self-renewal and pluripotent properties equivalent to those of ES cells [14–16]. Furthermore, the iPS cell technology enables the generation of individualized stem cells and thereby contributes to patient-oriented research, including developmental pathology,

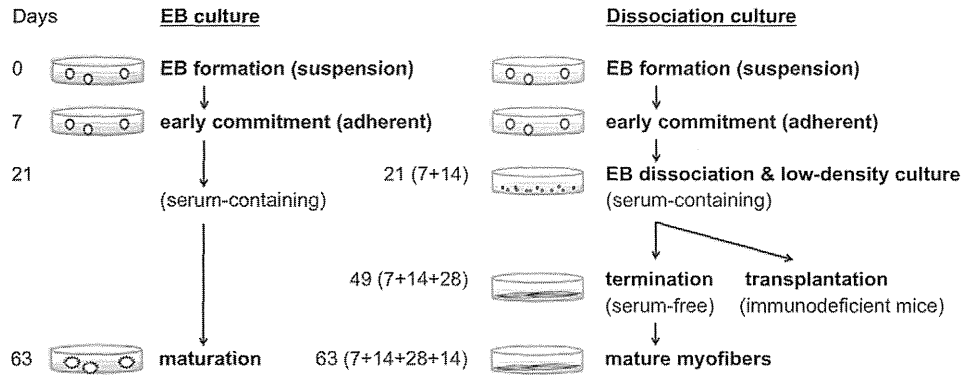

Figure 1. Schematic presentation of the differentiation protocol. Two different differentiation protocols were compared (Left: embryoid body (EB) culture, Right: Dissociation culture) and were exactly the same until the first 21 (7+14) days of culture. On the left side, EBs continued to be incubated in serum-containing medium without specific manipulation until the end of culture. On the right side, EBs and their outgrowth cells were dissociated and seeded onto collagen type I-coated tissue culture plates in serum-containing medium. The medium was changed to serum-free ITS medium on day 49 (7+14+28). In some experiments, the cells were harvested and used as donor cells for the transplantation assay at this time point.
doi:10.1371/journal.pone.0051638.g001

drug screening, and toxicity testing, which otherwise would be impossible in humans [17–18].

Thus far, several groups have demonstrated myogenic differentiation from human ES (hES) cells with different induction strategies [10,19]. The first approach is to induce lineage-specific differentiation by providing appropriate environmental factors, such as culture media, substrates, or cytokines. A classical approach is to induce myogenesis through the formation of three-dimensional cell aggregates called embryoid bodies (EBs), in which the differentiation processes of all 3 germ layers are recapitulated. Although it is an effective myogenic strategy employed for murine ES research [20,21], this method had not been successfully executed in human ES cells because of various difficulties [22], until recently [23,24]. However, the differentiation efficacy of these EB methods remains low and heterogeneous, and the potential of EB methods as a donor source for cell replacement therapy has not been investigated. Barberi et al. reported another two-dimensional culture protocol in which hES cells give rise to myogenic mesenchymal precursors. These precursor cells show efficient *in vitro* differentiation into skeletal myotubes and stable engraftment capacity *in vivo* [25,26]. However, from a practical perspective, this approach is difficult to use because it requires repetitive cell sorting to obtain a population of homogenous myogenic mesenchymal progenitors. Another approach to achieve myogenic differentiation is the use of genetic modification to directly activate myogenic signaling pathways. Forced expression of *MyoD* is known to transform fibroblasts to skeletal muscle cells [27], and is also applicable to murine ES cells [28]. Darabi et al. demonstrated that the forced expression of *PAX3* successfully induced paraxial mesodermal and subsequent myogenic differentiation in murine ES cells [29], and the induction of *PAX7* efficiently induced myogenesis both in human ES and iPS cells [30]. These methods are indeed effective myogenic strategies. However, genetic modification is accompanied by various concerns, such as potent tumorigenesis.

We previously reported on an EB-based culture method that induces efficient myogenesis from both murine ES and iPS cells, and described the purification of satellite-like cells and their persistent engraftment capacity *in vivo* [31,32]. The aims of this study were to 1) establish a novel *in vitro* culture system to induce efficient myogenesis from both human ES and iPS cells by modifying our EB-based method, without introducing any additional genes; and 2) investigate the capacity of the differentiated cells to engraft and repair damaged muscles *in vivo* to clarify whether they are an appropriate donor source in muscle regenerative medicine. Here, we describe a novel culture method for efficient myogenesis by using selective expansion of myogenic mesenchymal cells *in vitro* and demonstrate their capacity to engraft *in vivo*.

Materials and Methods

Maintenance of human ES and iPS cells

The hES cell line KhES1 was a kind gift from Dr. Norio Nakatsuji (Kyoto University, Kyoto, Japan) [33]. The hiPS cell lines 201B6, 201B7, 253G1, and 253G4 were established from human dermal fibroblasts by retrovirus-mediated transfection of 4 (201B6 and 201B7) or 3 (253G1 and 253G4) transcription factors (Oct3/4, Sox2, and Klf4, with or without c-Myc) [15,16]. The human ES and iPS cell lines were maintained on mitomycin-C (Kyowa Hakko Kirin, Tokyo, Japan)-treated SNL feeder cells in human ES cell maintenance medium [hESM: DMEM/F12 (Sigma-Aldrich, St. Louis, MO, USA) supplemented with 20% Knockout® Serum Replacement (Invitrogen, Carlsbad, CA, USA), 1% nonessential amino acid solution (Invitrogen), 5 mM sodium hydroxide solution, 100 μM 2-mercaptethanol, 2 mM L-glutamine] with 5 ng/ml basic fibroblast growth factor (R&D Systems, Minneapolis, MN, USA). The culture medium was changed daily. Colonies were passaged every 4 or 5 days.

The human ES and iPS cell lines were used in conformity with The Guidelines for Derivation and Utilization of Human Embryonic Stem Cells of the Ministry of Education, Culture, Sports, Science and Technology, Japan.

Skeletal muscle differentiation

EB culture (Figure 1, Left): Undifferentiated human ES and iPS cells were trypsinized and floated in hESM as clusters for 7 days to form EBs. These EBs were then transferred to 0.1% gelatin-coated tissue culture plates and cultured in ITS medium [DMEM supplemented with ITS-X (Invitrogen), nonessential amino acids (Invitrogen), Glutamax® supplement (Invitrogen), and 100 μM 2-mercaptoethanol (Wako, Osaka, Japan)] for 14 days. Afterwards, the medium was changed to skeletal muscle induction medium [SkIM: high-glucose DMEM supplemented with 10% fetal calf serum (FCS; Invitrogen), 5% horse serum (HS; Sigma), nonessential amino acids (Invitrogen), and 100 μM 2-mercaptoethanol (Wako)]. The cells were analyzed on days 7, 21, 35, 49, 63, 84, and 112. The medium was changed every 3 to 4 days.

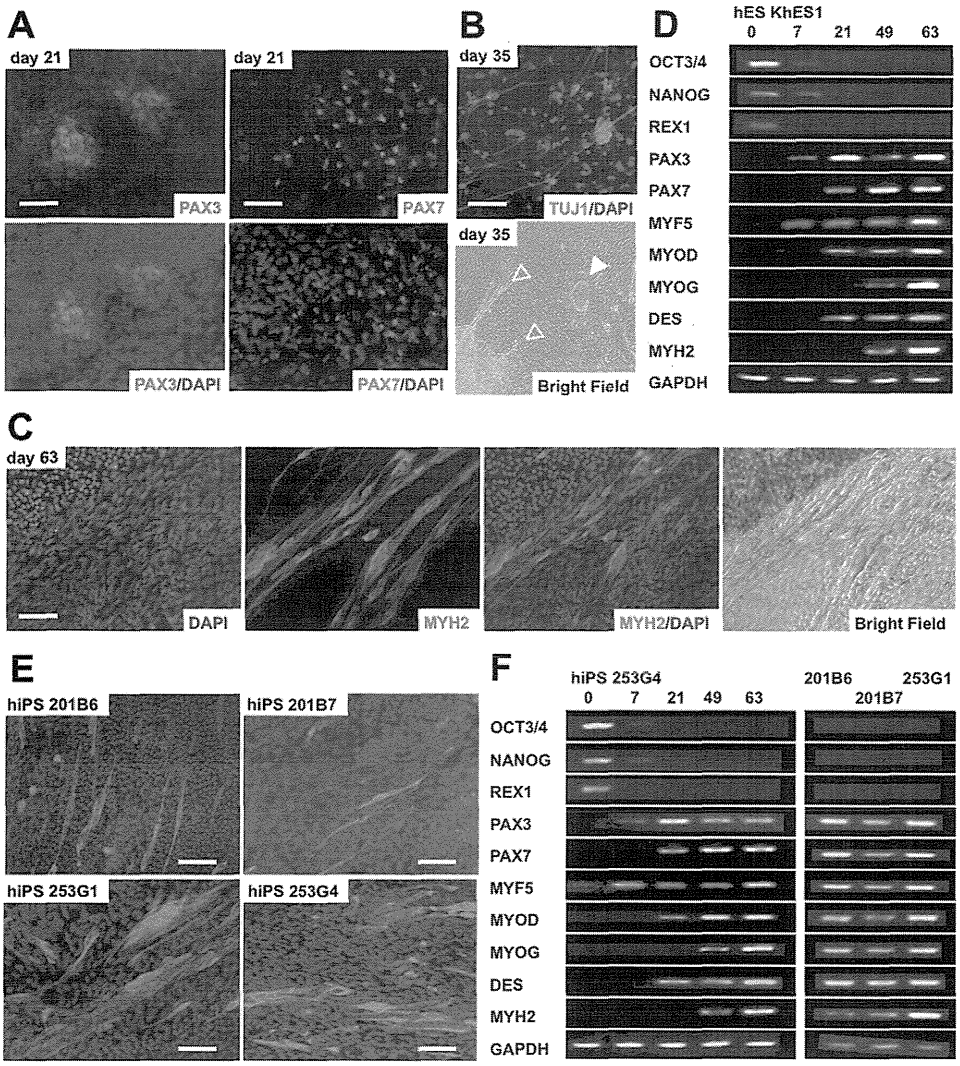

Figure 2. Skeletal muscle development from human embryonic stem (hES) and human induced pluripotent stem (hiPS) cells by the EB culture method. (A) PAX3- and PAX7-positive nuclei emerged in the proximal area of the embryoid body (EB)-outgrowth cells derived from hES KhES1 cells. (B) Simultaneous derivation of neural and cardiac cells in the EB-outgrowth cells derived from hES KhES1 cells. Upper: TUJ1-positive neural cells observed on day 7+28. Lower: Neural cells (outlined arrowheads) and colonies of beating cardiomyocytes (white arrowhead) appeared on day 7+28. (C) Skeletal myosin-positive myofibers in the EB-outgrowth cells derived from human embryonic stem (hES) KhES1 cells detected on day 7+42. (D) Sequential analysis of undifferentiated and skeletal myogenesis-related gene expression by semi-quantitative RT-PCR. (E) Skeletal myosin-positive fibers from human induced pluripotent stem (hiPS) cells. Four hiPS cell-lines were used. hiPS 201B6 on day 7+105, hiPS 201B7 on day 7+105, hiPS 253G1 on day 7+77, and hiPS 253G4 on day 7+56. (F) Sequential analysis of undifferentiated and skeletal myogenesis-related gene expression by semi-quantitative RT-PCR. In (A-C) and (E), antibodies were visualized using Cy3 (red). Nuclei were counterstained with DAPI (blue). Scale bars = 100 μm.
doi:10.1371/journal.pone.0051638.g002

Dissociation culture (Figure 1, Right): In some experiments, EBs and their outgrowth cells were treated with 0.25% trypsin/EDTA on day 21 and seeded onto collagen type I-coated tissue culture plates (BD Bioscience, Bedford, MA, USA) at a density of 3000 cells/cm^2 in SkIM. On day 49, the medium was changed to ITS medium. For obtaining mature myofibers, cells were cultivated for up to 70 days. The differentiated cells were analyzed on days 7, 21, 49, 56, 63, and 70.

Complementary DNA (cDNA) synthesis and reverse transcription-polymerase chain reaction (RT-PCR)

Cells were trypsinized on the indicated days of differentiation. Total RNA samples were extracted using silica gel membrane-based spin columns (RNeasy Mini-Kit®, Qiagen, Valencia, CA, USA). cDNA samples were synthesized using the Ominscript-RT Kit® (Qiagen) and used for subsequent PCR. All procedures were performed according to the manufacturer's instructions. The cDNA templates were initially denatured at 94°C for 5 min, followed by 35 amplification reactions consisting of 94°C for 30 seconds (denaturing), 55–60°C for 30 seconds (annealing), and 72°C for 60 seconds (extension), with a final extension at 72°C for 7 min. Oligonucleotide primers were designed for Oct3/4, Nanog, Pax3, Pax7, Myf5, MyoD, Myogenin, Desmin, TUBB3, TNNI3, and GAPDH. The primer sequences and temperature settings are described in supplemental materials (Table S1).

Flow cytometric (FCM) analysis

Staining procedures, FCM analysis, and cell sorting were performed as described previously [31,32]. Cells trypsinized on the

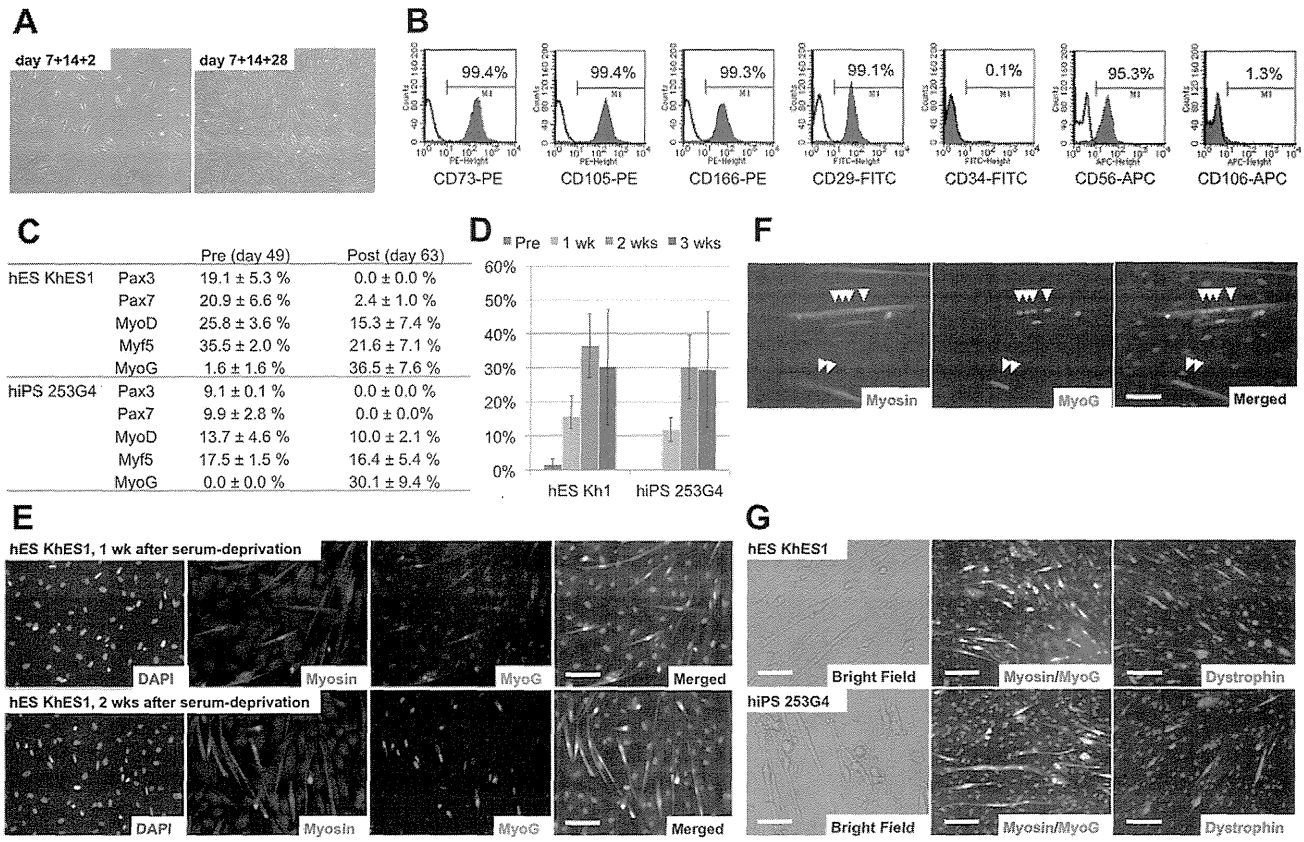

Figure 3. Characterization and differentiation of the derived myogenic mesenchymal cells. (A) Morphology of the derived myogenic mesenchymal progenitors 2 days (day 7+14+2) and 4 weeks (day 7+14+28) after replating. Homogeneous spindle-shaped fibroblastic cells were observed. (B) Surface marker analysis of myogenic mesenchymal progenitors. Representative data from KhES1 differentiation are shown. Note that CD56 in addition to mesenchymal markers CD73, CD105, CD166, and CD29 was exclusively expressed. (C) Changes in the expression of myogenic markers were analyzed by immunofluorescence. The number of Cy3-positive nuclei was divided by the total number of nuclei stained by DAPI. The expression of myogenic progenitor markers decreased after exposure to serum-free medium, whereas the number of MYOG-positive cells substantially increased after serum deprivation. (D) Changes in the number of MYOG-positive nuclei were observed up to 3 weeks after serum deprivation. hES/iPS-derived myofibers tended to detach from tissue culture plates during long-term culture in serum-free medium. (E) Serum deprivation increased the number of skeletal myosin-positive fibers and MYOG-positive nuclei for more than 2 weeks. KhES1 was used in this figure. (F) Multinucleated myofibers denoted by MYOG myogenin-positive nuclei aligned in skeletal myosin-positive fibers. (G) Morphology of mature myofibers, which were stained with skeletal myosin, MYOG, and dystrophin, from both KhES1 and 253G4 cells. Skeletal myosin was visualized with fluorescein isothiocyanate (FITC) (Green), myogenin was visualized with Cy3 (red), and nuclei were counterstained with DAPI (blue). Scale bars = (C, E) 100 μm, (D) 50 μm.
doi:10.1371/journal.pone.0051638.g003

indicated days of differentiation were stained with phycoerythrin- or allophycocyanin-conjugated primary antibodies (Abs). Abs used for FCM analysis included mouse anti-CD73, anti-CD105, anti-CD166, anti-CD34, anti-CD56, anti-CD106 (BD Bioscience), and anti-CD29 (Beckman Coulter, Brea, CA, USA). Dead cells were excluded by propidium iodide (Sigma). Samples were analyzed using FACSCalibur (BD Bioscience) and Cell Quest software (BD Bioscience).

Immunostaining assays

Immunofluorescence analyses were performed as previously described [31,32]. Briefly, samples were fixed for 5 min in 4% paraformaldehyde (PFA) and then permeabilized with 0.1% Triton X-100 in phosphate-buffered saline (PBS) for 10 min. After incubation in 2% skim milk for 1 h at room temperature to block nonspecific antibody binding, cells were incubated with primary antibodies for 1 h at room temperature. The primary antibodies used in this study were as follows: mouse anti-Pax3 (R&D Systems, Minneapolis, MN, USA), mouse anti-Pax7 (R&D Systems), rabbit anti-Myf5 (Santa Cruz Biotechnology, Inc., Santa Cruz, CA, USA), mouse anti-MyoD1, mouse anti-myogenin (Dako, Carpinteria, CA, USA), mouse anti-fast twitch myosin heavy chain (MYH2) (MY32; Zymed Laboratories, San Francisco, CA, USA), rabbit anti-skeletal myosin (Sigma), mouse anti-dystrophin (MANDRA1; Sigma), rabbit anti-laminin (Dako), mouse anti-human merosin (Laminin alpha 2), mouse anti-human lamin A/C (Novocastra Laboratories, Newcastle-upon-Tyne, UK), mouse anti-beta-tubulin III (TUJ1) (Sigma), and rabbit anti-glial fibrillary acidic protein antibody (GFAP) (Sigma). After washing twice with PBS, samples were incubated with secondary antibodies for 1 h at room temperature. The secondary antibodies used in this study were Cy3-conjugated anti-mouse IgG (Jackson ImmunoResearch Laboratories Inc., West Grove, PA, USA) and fluorescein isothiocyanate (FITC)-conjugated anti-rabbit IgG (Jackson ImmunoResearch). DAPI was used for nuclear staining. These samples were then examined using fluorescent microscopes (FluoView System; Olympus, Tokyo, Japan). Photographs were acquired with an Axio-Cam (Carl Zeiss Vision, Hallbergmoos,

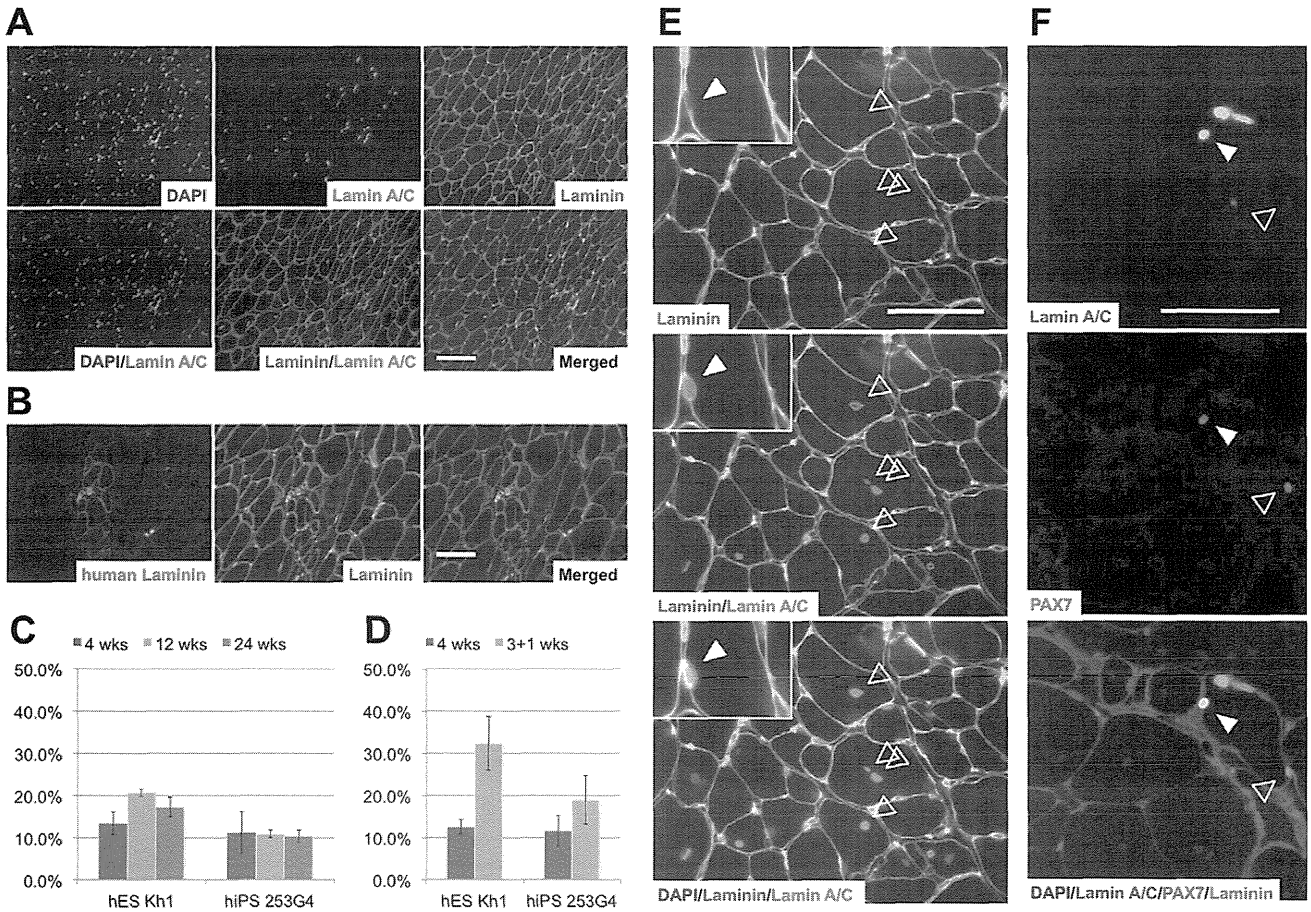

Figure 4. Engraftment of myogenic progenitors in damaged muscles of immunodeficient mice. (A) Human nuclei labeled with human-specific lamin A/C localized mainly inside muscle fibers surrounded by laminin. (B) Muscle reconstruction by transplanted human cells was demonstrated by the detection of human-specific laminin-alpha 2. (C) The proportion of myofibers containing human nuclei at 4, 12, and 24 weeks after transplantation. (D) The proportion of myofibers containing human nuclei in reinjured (3+1 weeks) and in non-reinjured mice (4 weeks) at 4 weeks after transplantation. In C and D, data are presented as the mean ± standard deviation. (E) Distribution of the transplanted cells at 24 weeks after transplantation. Typical central nuclei of human origin were observed (outlined arrowheads). Some human cells located within the lamina rara beneath the basal lamina, indicating engraftment of the transplanted cells into a satellite cell compartment (white arrowhead). (F) Triple-staining for human Lamin A/C, PAX7, and pan-Laminin clearly demonstrated the existence of PAX7-positive human nuclei indicating the transplanted cells engrafted as satellite cells (white arrowhead). Human lamin A/C-negative host satellite cells were also detected (outlined arrowhead). Laminin was stained by a polyclonal antibody that recognizes both human and murine laminin, and was subsequently visualized with fluorescein isothiocyanate (FITC) (Green); human lamin A/C and human-specific laminin, with Cy3 (red). Nuclei were counterstained with DAPI (blue). Scale bars = (A) 100 μm, (B) and (E) 50 μm.
doi:10.1371/journal.pone.0051638.g004

Germany). To quantify myogenic transcription factor-positive cells, we counted the number of Cy3-positive nuclei and divided this value by the total number of nuclei stained by DAPI.

For triple staining, we modified the protocol described by Darabi and his colleagues [30]. Briefly, samples were fixed for 20 min in 4% PFA, followed by permeabilization using 0.3% Triton X-100 in PBS. After incubation in blocking solution consisting of a mixture (1:1) of 3% bovine serum albumin (Invitrogen) and MOM blocking agent (Vector Laboratories Inc., Burlingame, CA, USA) for 1 h at room temperature, the slides were incubated with mouse anti-Pax7 (R&D Systems). After washing twice with PBS, samples were incubated with alexa-fluor 555 conjugated anti-mouse IgG (Invitrogen) for 30 min. After washing twice, the slides were blocked using the same solution for 1 h at room temperature. Subsequently, the slides were incubated with mouse anti-human Lamin A/C (Novocastra) and rabbit anti-laminin (DAKO) for 1 h at room temperature, followed by incubation with alexa fluor 488-conjugated anti-mouse IgG and alexa fluor 647-conjugated anti-rabbit IgG (Jackson Immunoresearch). The nuclei were counter-stained using DAPI and analyzed by AS-MDW system (Leica Microsystems GmbH, Wetzlar, Germany).

Transplantation

Eight-week-old male immunodeficient NOD/Shi-scid/IL-2Rγ^{null} (NOG) mice (Central Laboratories for Experimental Animals, Kanagawa, Japan) [34] were used as host mice to avoid immunological rejection. Host tibialis anterior (TA) muscles were bilaterally injected with 50 μL of 10 μM cardiotoxin (CTX; Latoxan, Valence, France) to induce muscle degeneration 24 h before transplantation. These mice were systemically irradiated to block endogenous muscle regeneration. Irradiation was delivered in 2 fractions of 1.2 Gy, a sub-lethal dose for NOG mice. The cells (1.0×10^5 or 5.0×10^5) were suspended in 20 μL of medium and directly injected into the pre-damaged left TA muscles. The same amount of medium was injected into the right TA muscles, which served as the control. Mice were sacrificed at 4, 12, and 24 weeks